Supporting Information for the Paper Entitled,

Terminal Titanyl Complexes of Tri- and Tetrametaphosphate: Synethesis, Structures, and Reactivity with Hydrogen Peroxide

Julia M. Stauber, and Christopher C. Cummins*

Department of Chemistry, Massachusetts Institute of Technology, 77 Massachusetts Avenue, Cambridge, Massachusetts 02139

E-mail: ccummins@mit.edu

Contents

*To whom correspondence should be addressed

1 Spectroscopic characterization of Ti(IV) metaphosphate complexes.

1.1 $[PPN]_4[OTiP_4O_{12}]_2$ ($[PPN]_4$[1]).

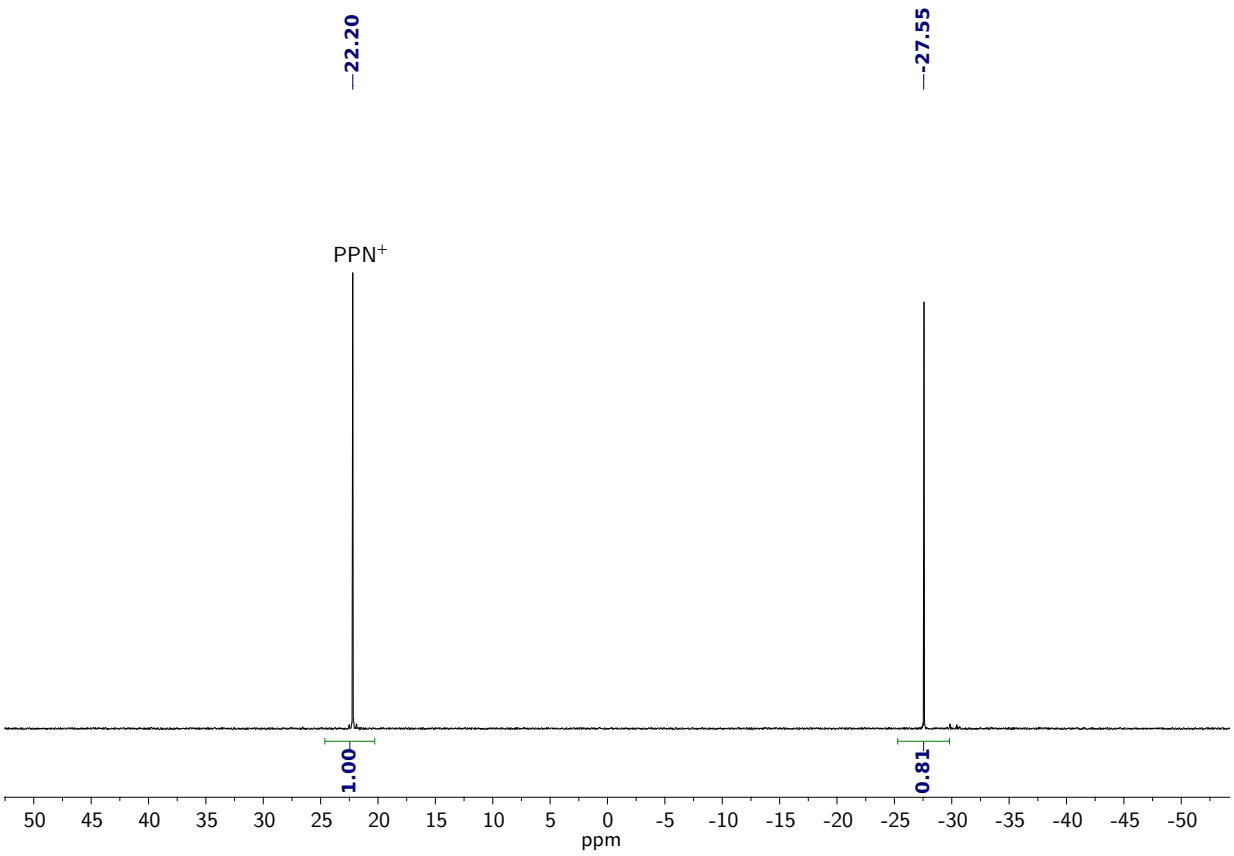

Figure S1: $^{31}P\{^1H\}$ NMR spectrum of $[PPN]_4$[**1**] (CD_3CN, 162 MHz, 25 °C).

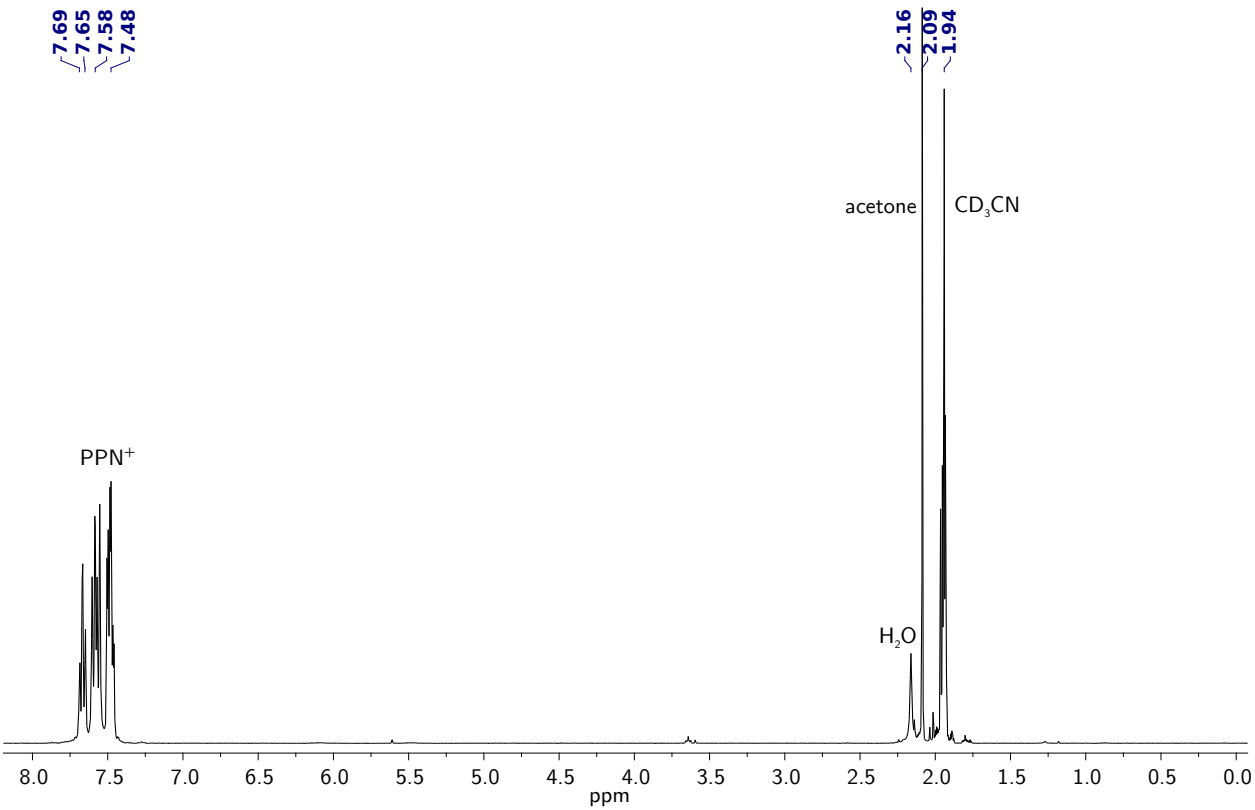

Figure S2: ^{1}H NMR spectrum of [PPN]$_4$[**1**] (CD_3CN, 400 MHz, 25 °C).

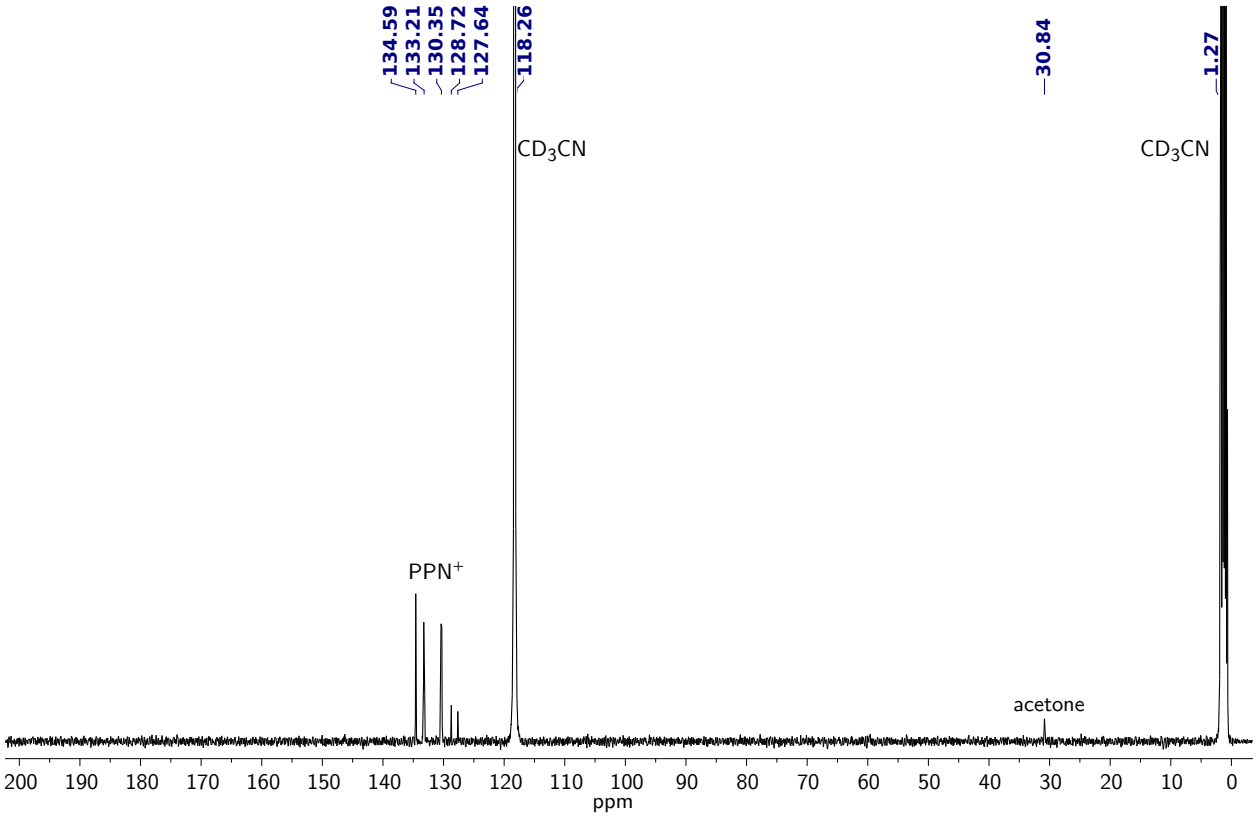

Figure S3: $^{13}C\{^{1}H\}$ NMR spectrum of $[PPN]_4$[**1**] (CD_3CN, 101 MHz, 25 °C).

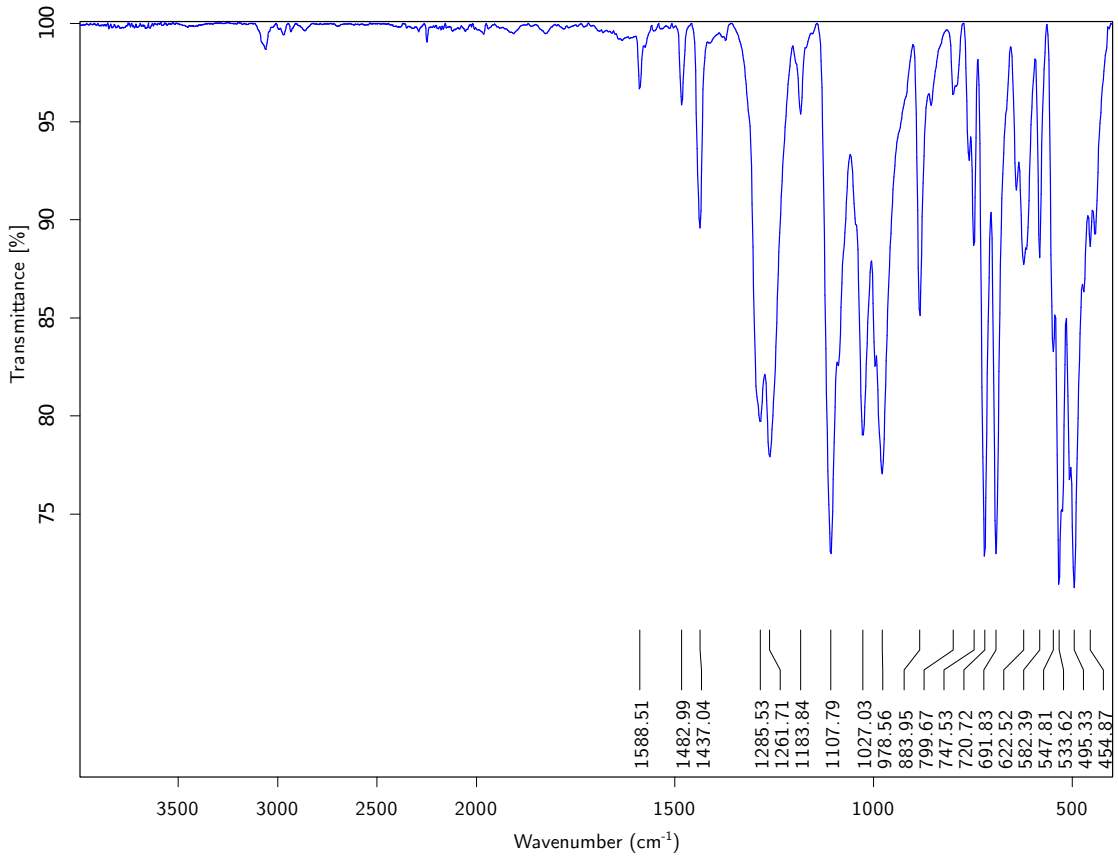

Figure S4: ATR-IR of $[PPN]_4$[**1**].

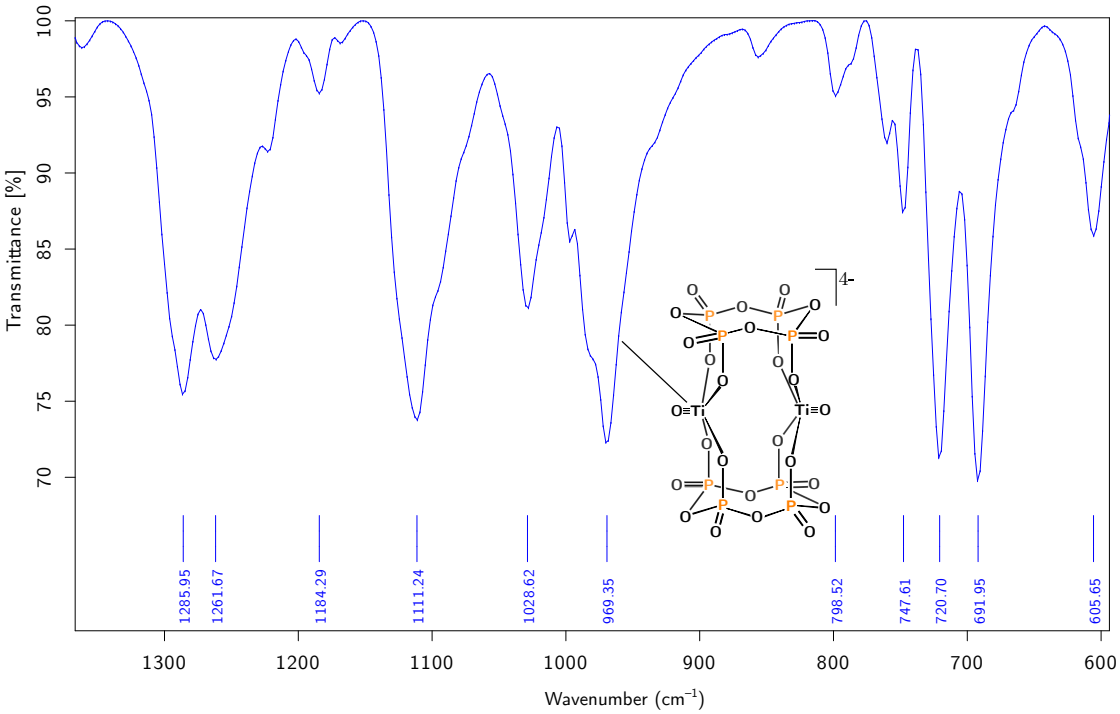

Figure S5: Zoomed-in ATR-IR of $[PPN]_4$[**1**].

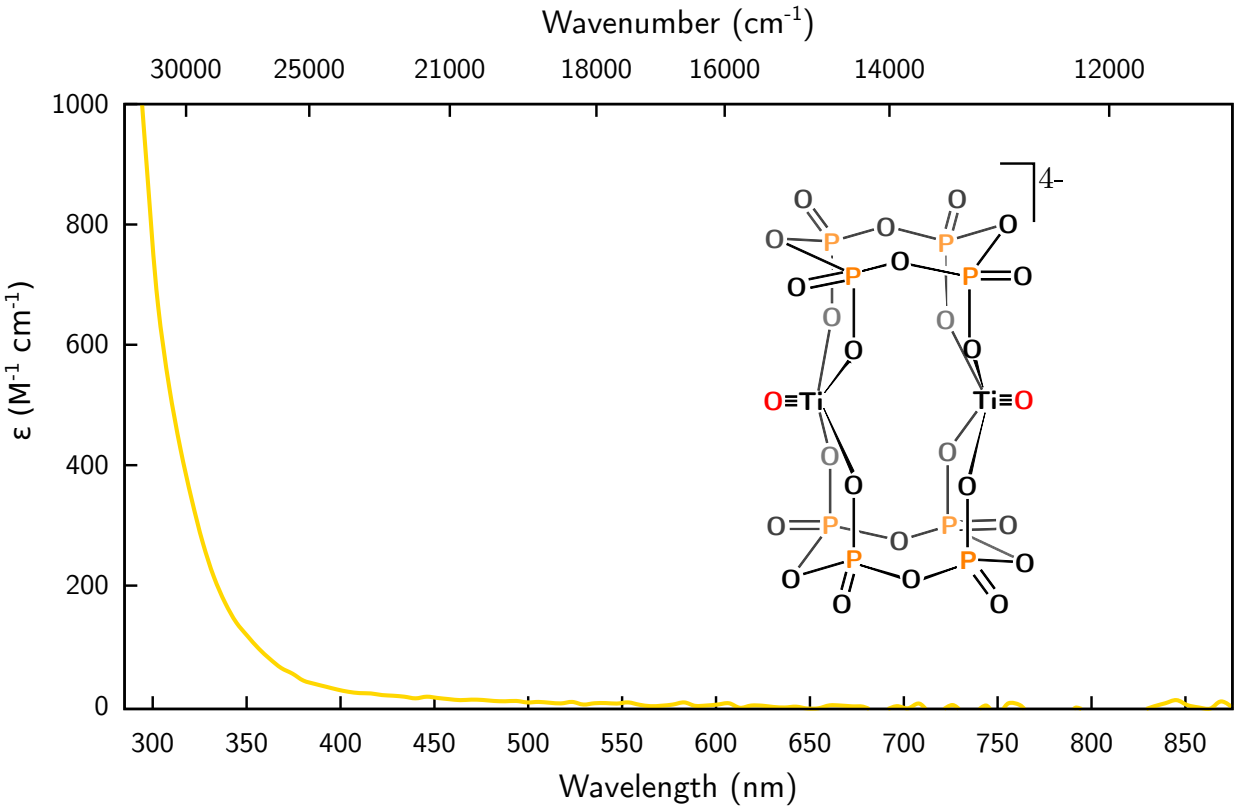

Figure S6: UV-Vis spectrum of $[PPN]_4$[**1**] (0.5 mM, MeCN, 20 °C).

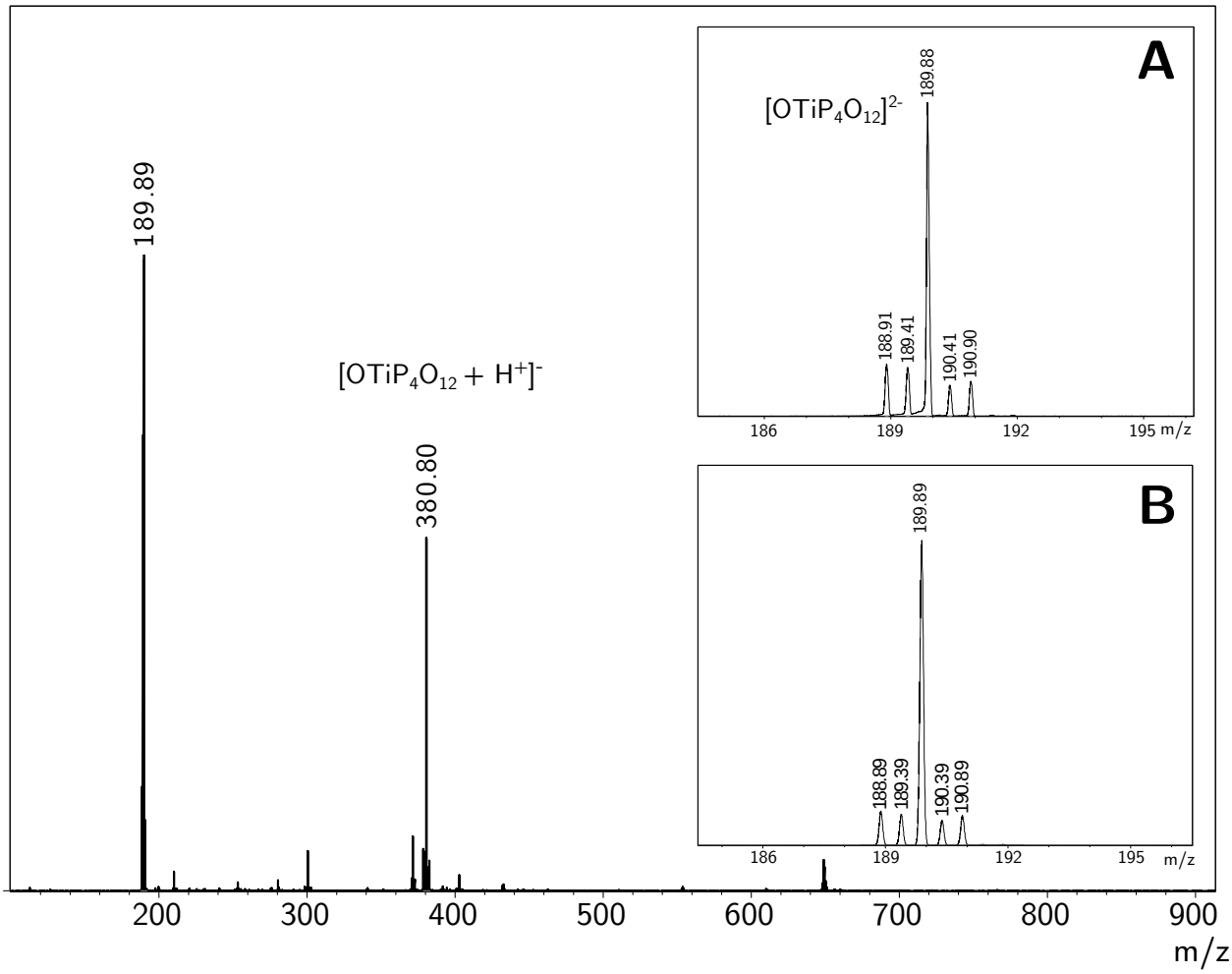

Figure S7: ESI-MS(–) of $[PPN]_4$[**1**]. **A**: Zoomed-in spectrum; **B**: simulated spectrum (MeCN, 3200 V).

1.2 $[PPN]_2[OTiP_3O_9(acac)]$ ($[PPN]_2$[2]).

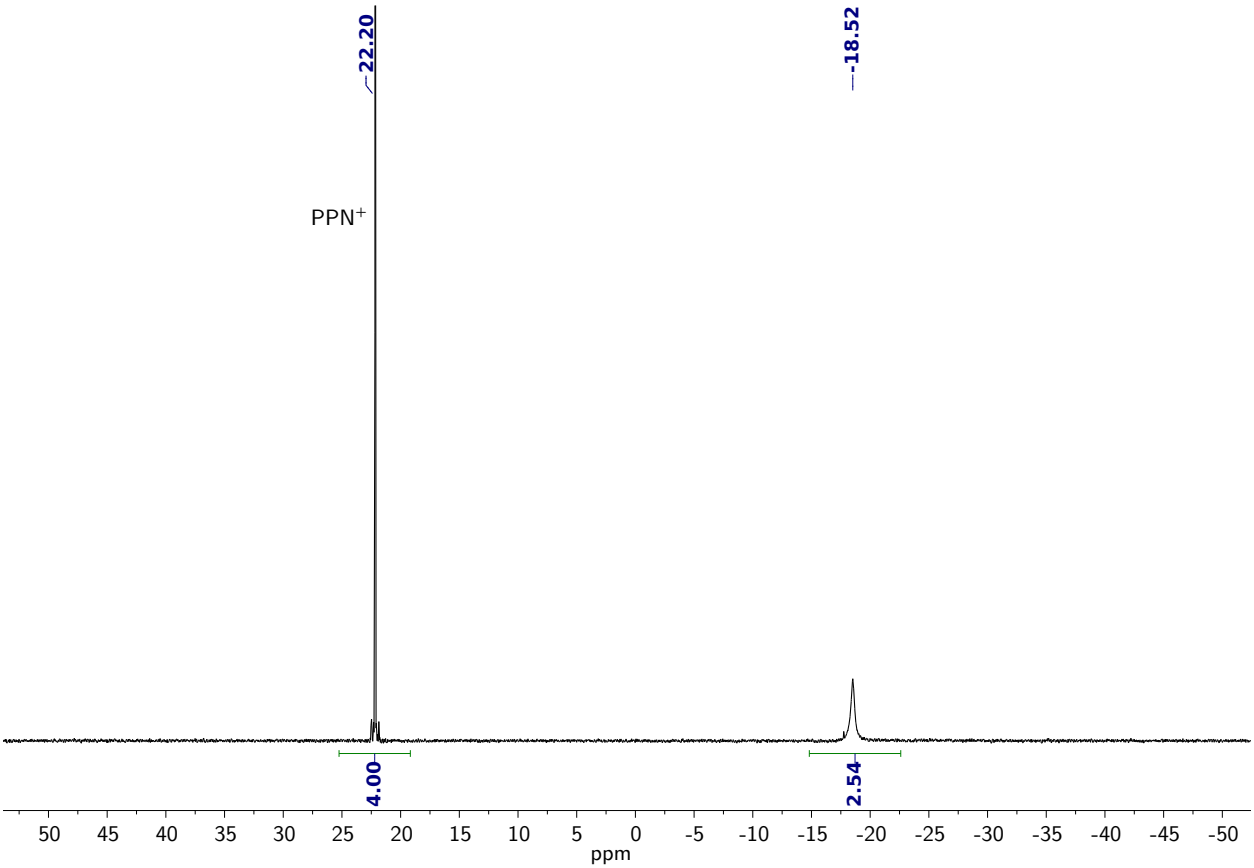

Figure S8: $^{31}P\{^1H\}$ NMR spectrum of $[PPN]_2$[**2**] (CD_3CN, 162 MHz, 25 °C).

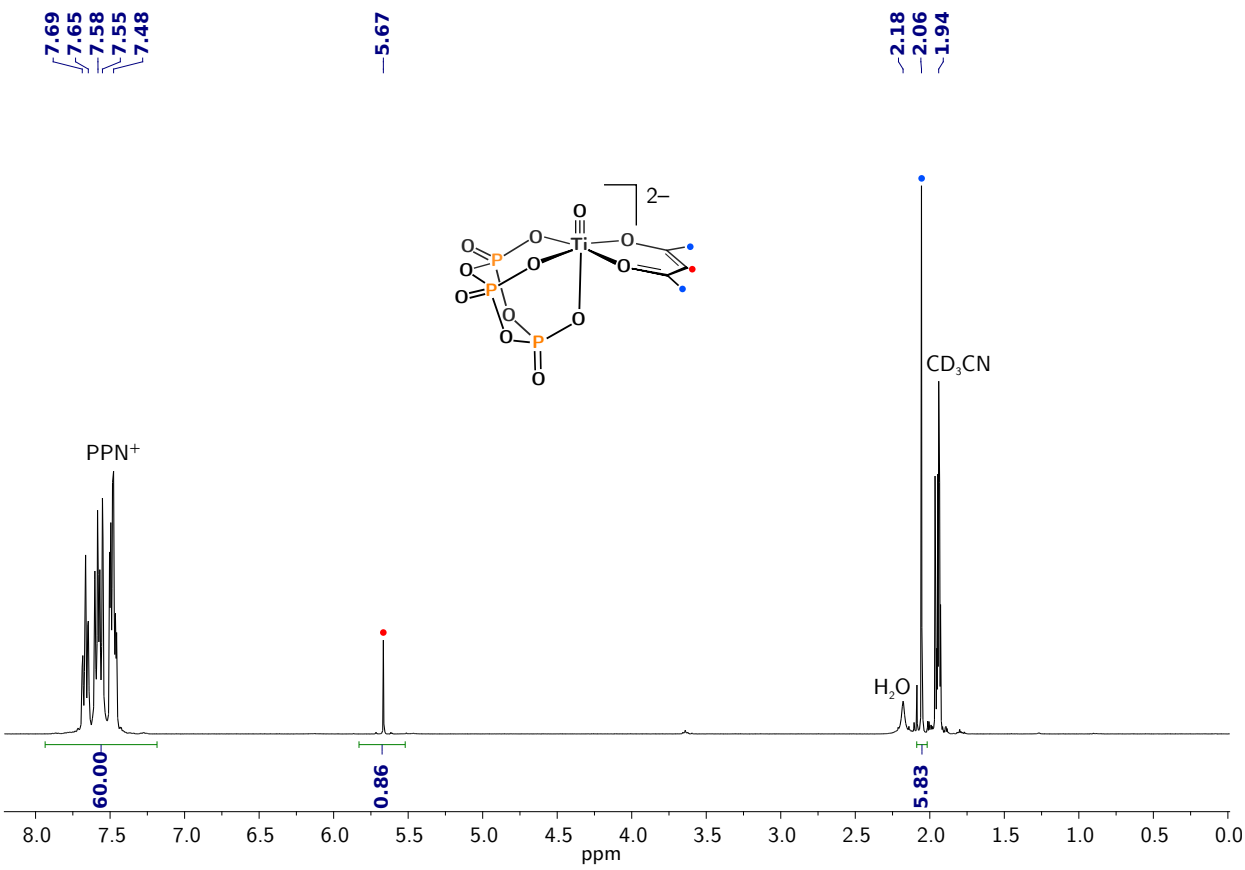

Figure S9: ^{1}H NMR spectrum of $[PPN]_2$[**2**] (CD_3CN, 400 MHz, 25 °C).

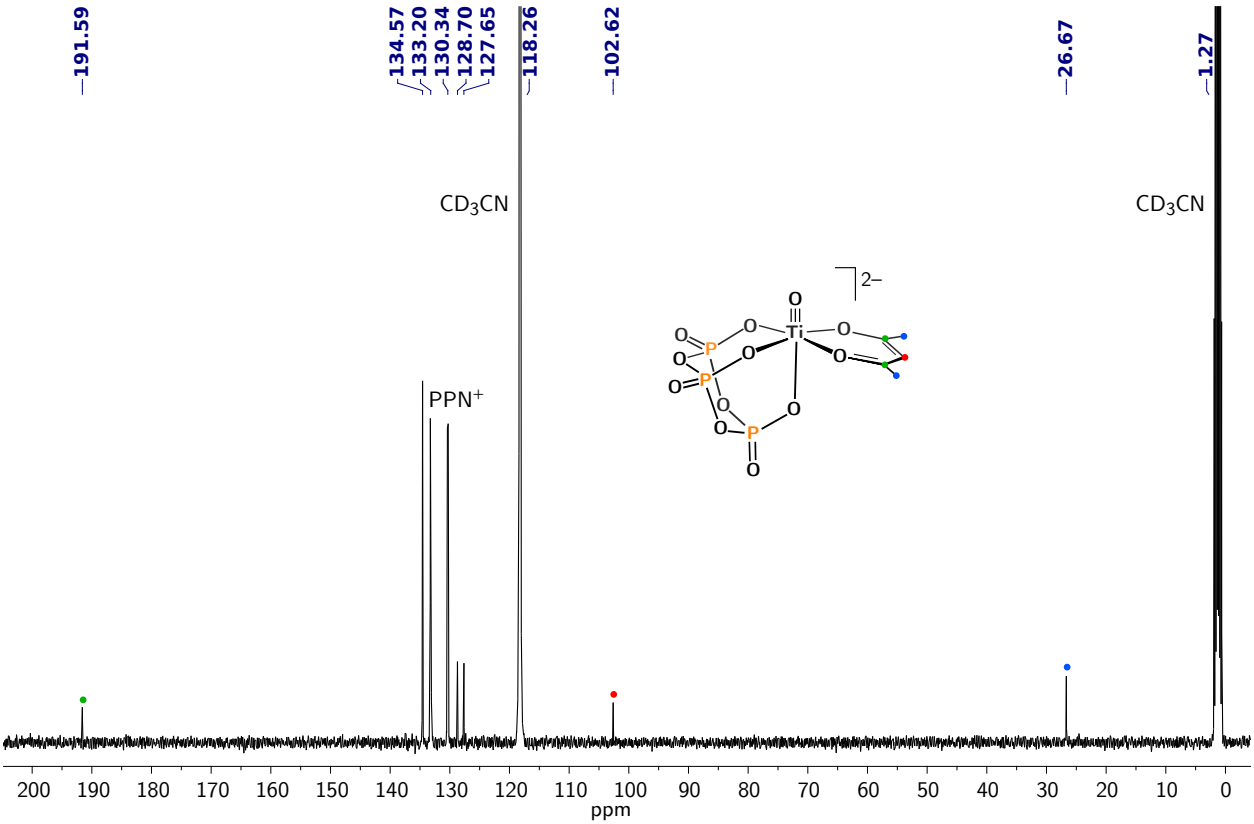

Figure S10: $^{13}C\{^{1}H\}$ NMR spectrum of $[PPN]_2$[**2**] (CD_3CN, 101 MHz, 25 °C).

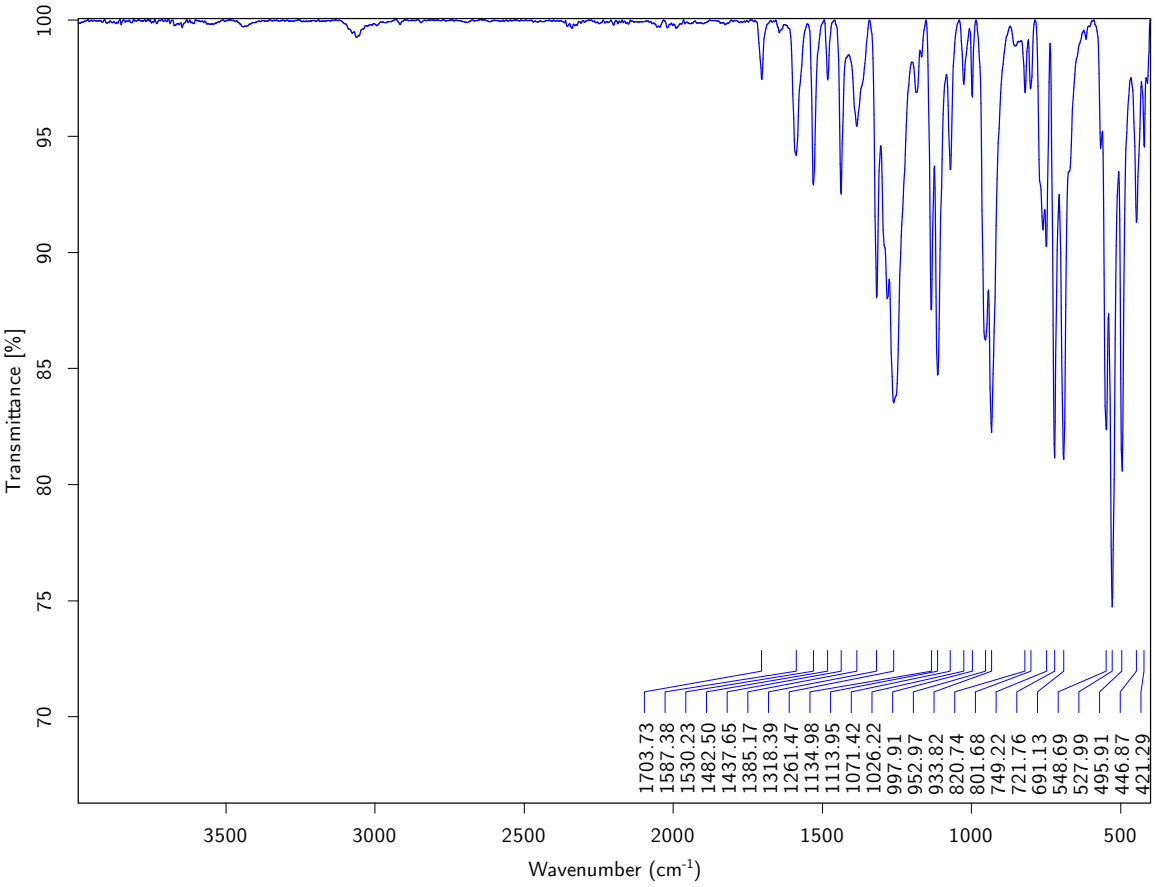

Figure S11: ATR-IR of $[PPN]_2$[**2**].

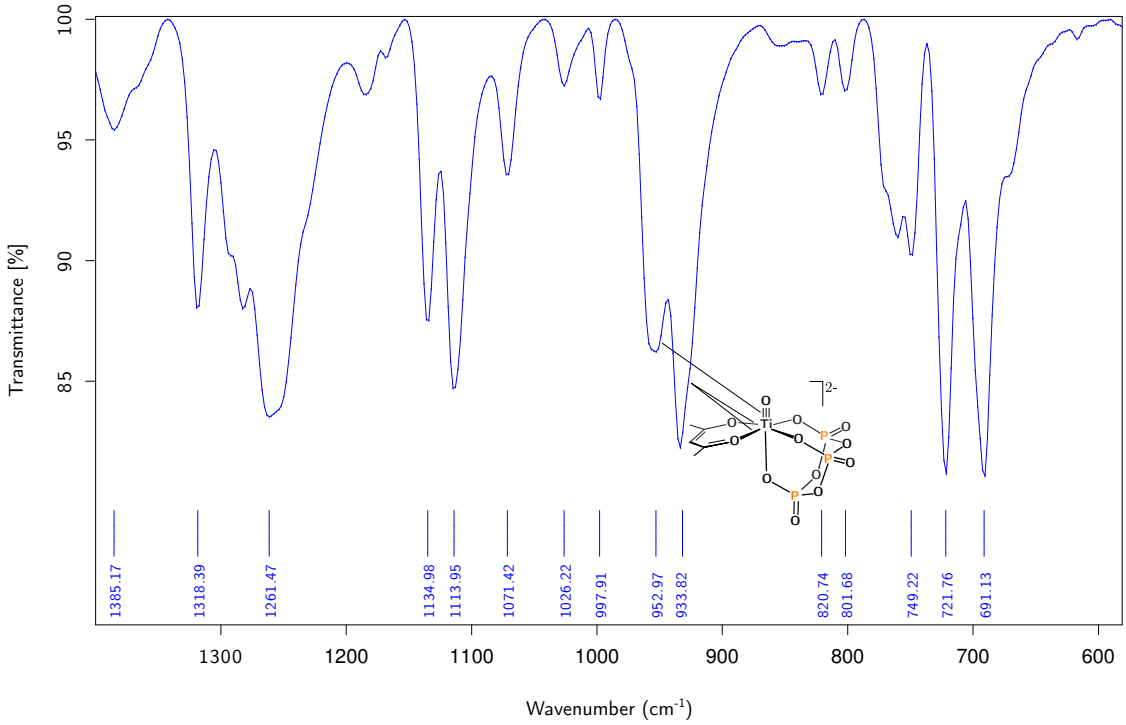

Figure S12: Zoomed-in ATR-IR of $[PPN]_2$[**2**].

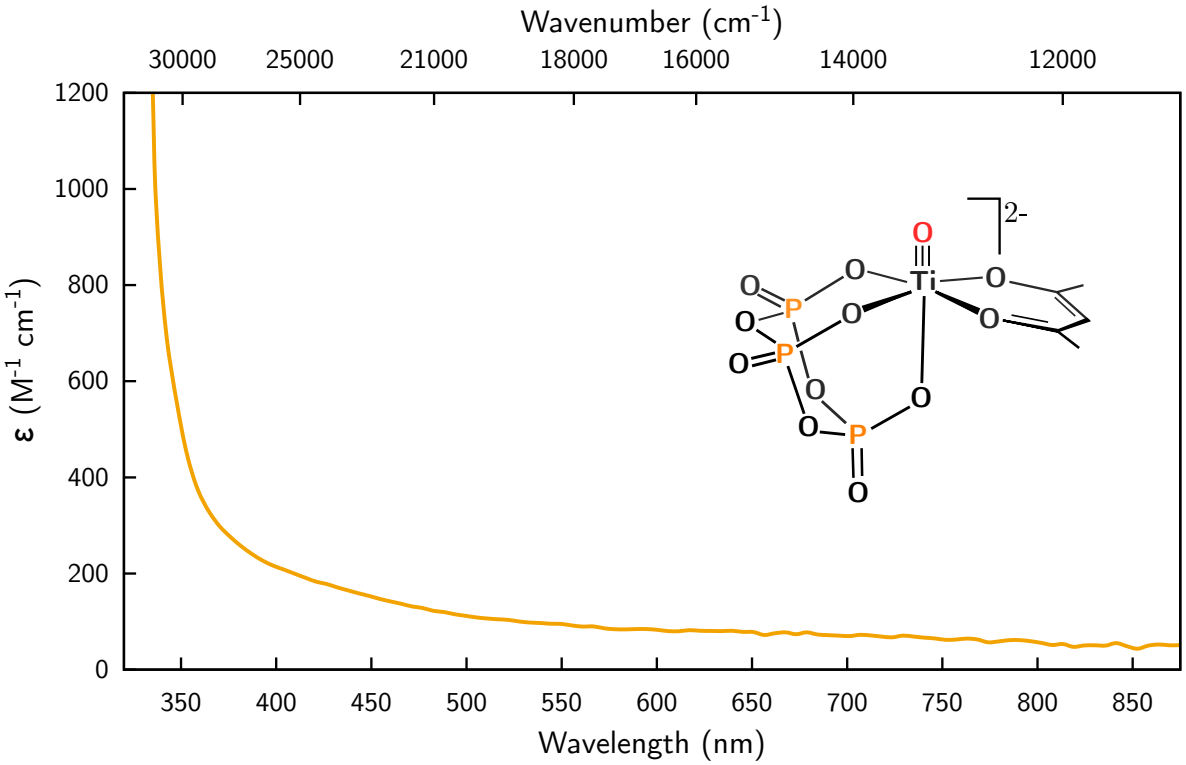

Figure S13: UV-Vis spectrum of $[PPN]_2$[**2**] (1.0 mM, MeCN, 20 °C).

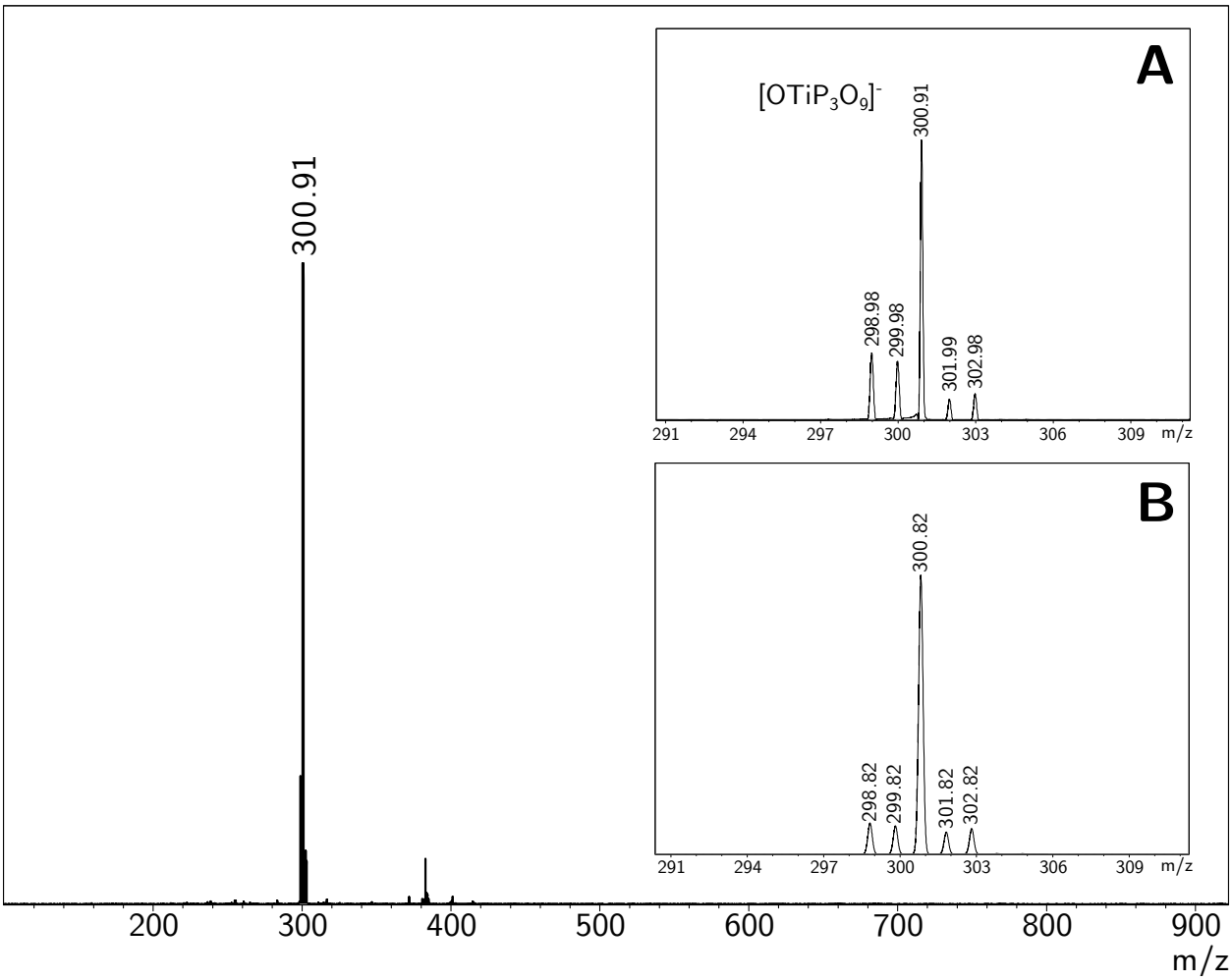

Figure S14: ESI-MS(–) of $[PPN]_2$[**2**]. **A**: Zoomed-in spectrum; **B**: simulated spectrum (MeCN, 3200 V). The acac ligand is not observable under ESI-MS(–) conditions.

1.3 $[PPN]_4[O_2TiP_4O_{12}]_2$ ($[PPN]_4$[3]).

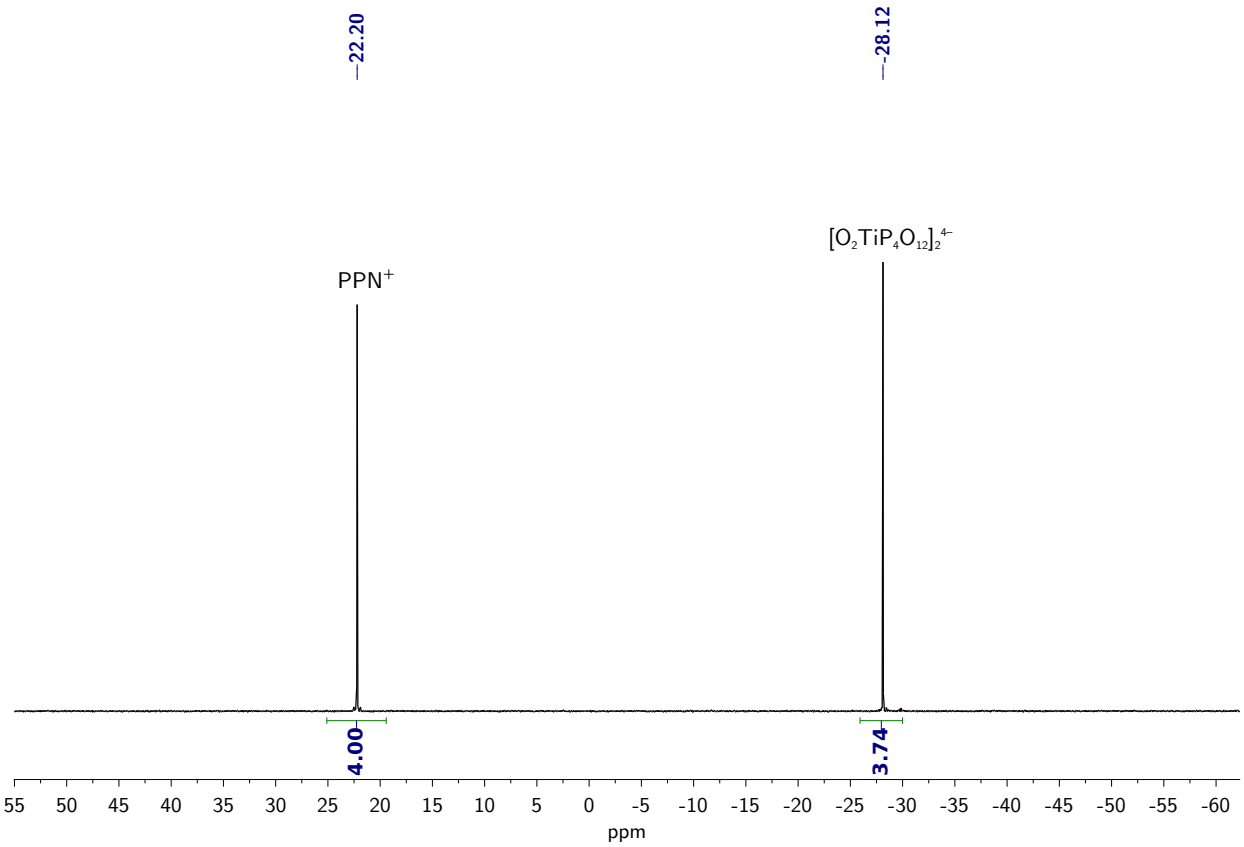

Figure S15: $^{31}P\{^1H\}$ NMR spectrum of $[PPN]_4$[**3**] (CD_3CN, 162 MHz, 25 °C).

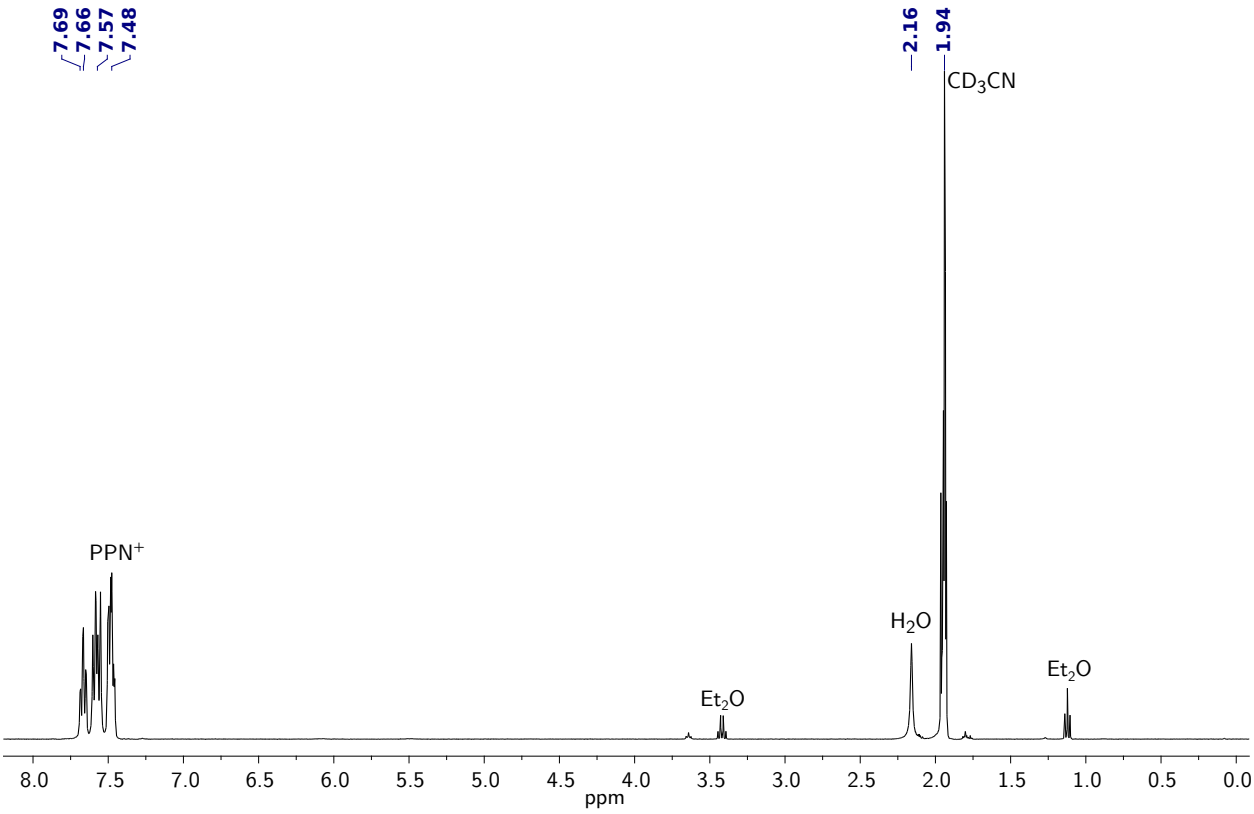

Figure S16: ^{1}H NMR spectrum of [PPN]$_4$[**3**] (CD_3CN, 400 MHz, 25 °C).

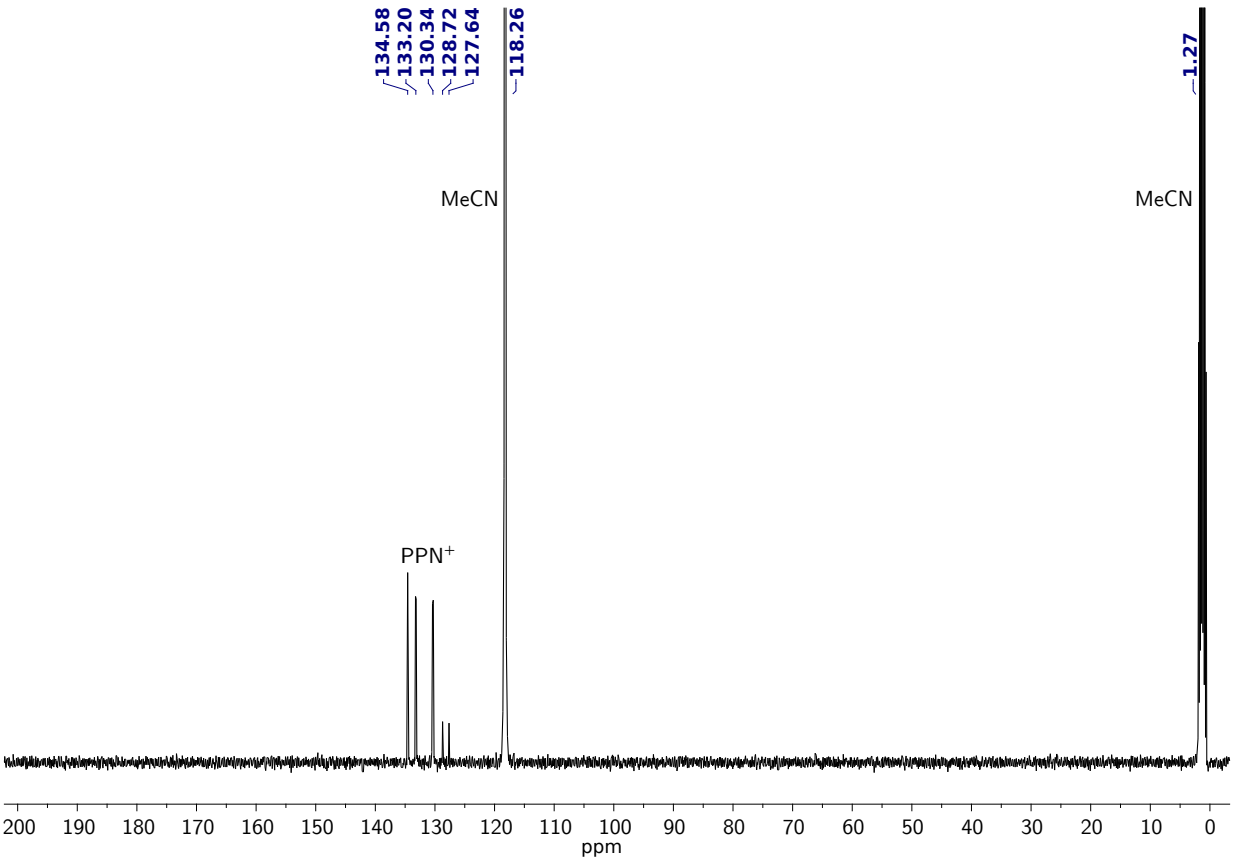

Figure S17: $^{13}C\{^{1}H\}$ NMR spectrum of $[PPN]_4$[**3**] (CD_3CN, 101 MHz, 25 °C).

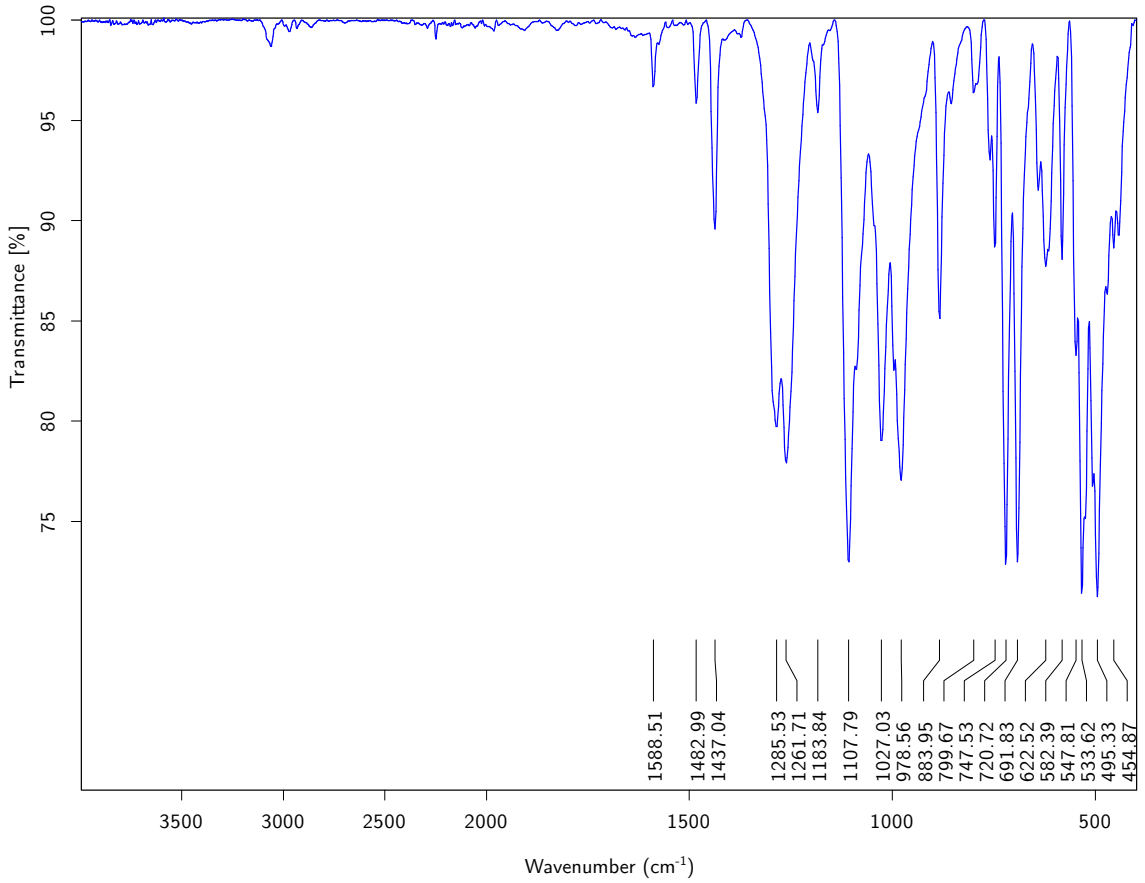

Figure S18: ATR-IR of $[PPN]_4$[**3**].

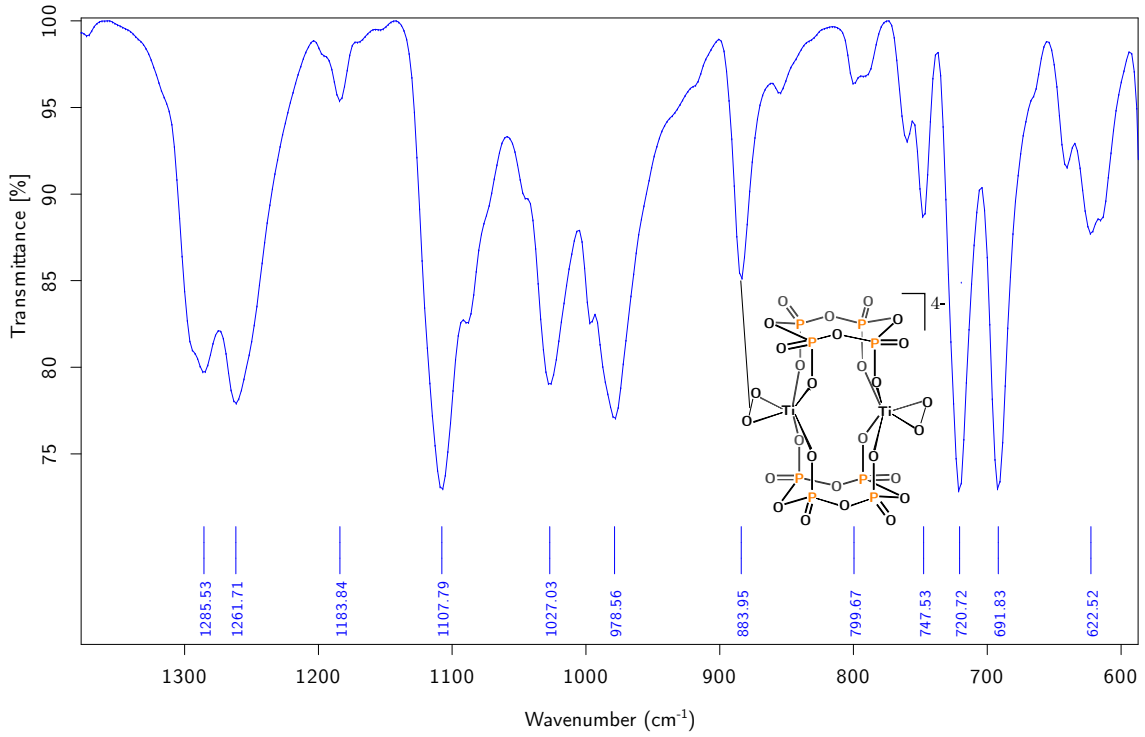

Figure S19: Zoomed-in ATR-IR of $[PPN]_4$[**3**].

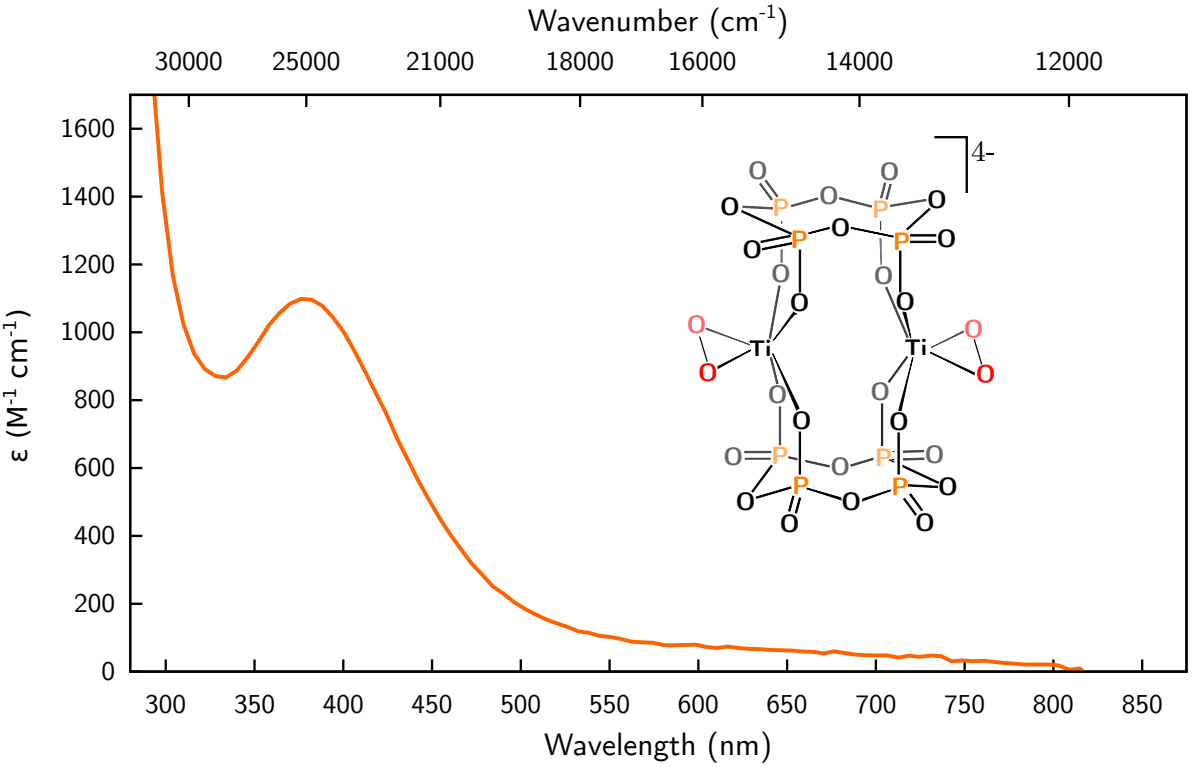

Figure S20: UV-Vis spectrum of $[PPN]_4$[**3**] (0.5 mM, MeCN, 20 °C).

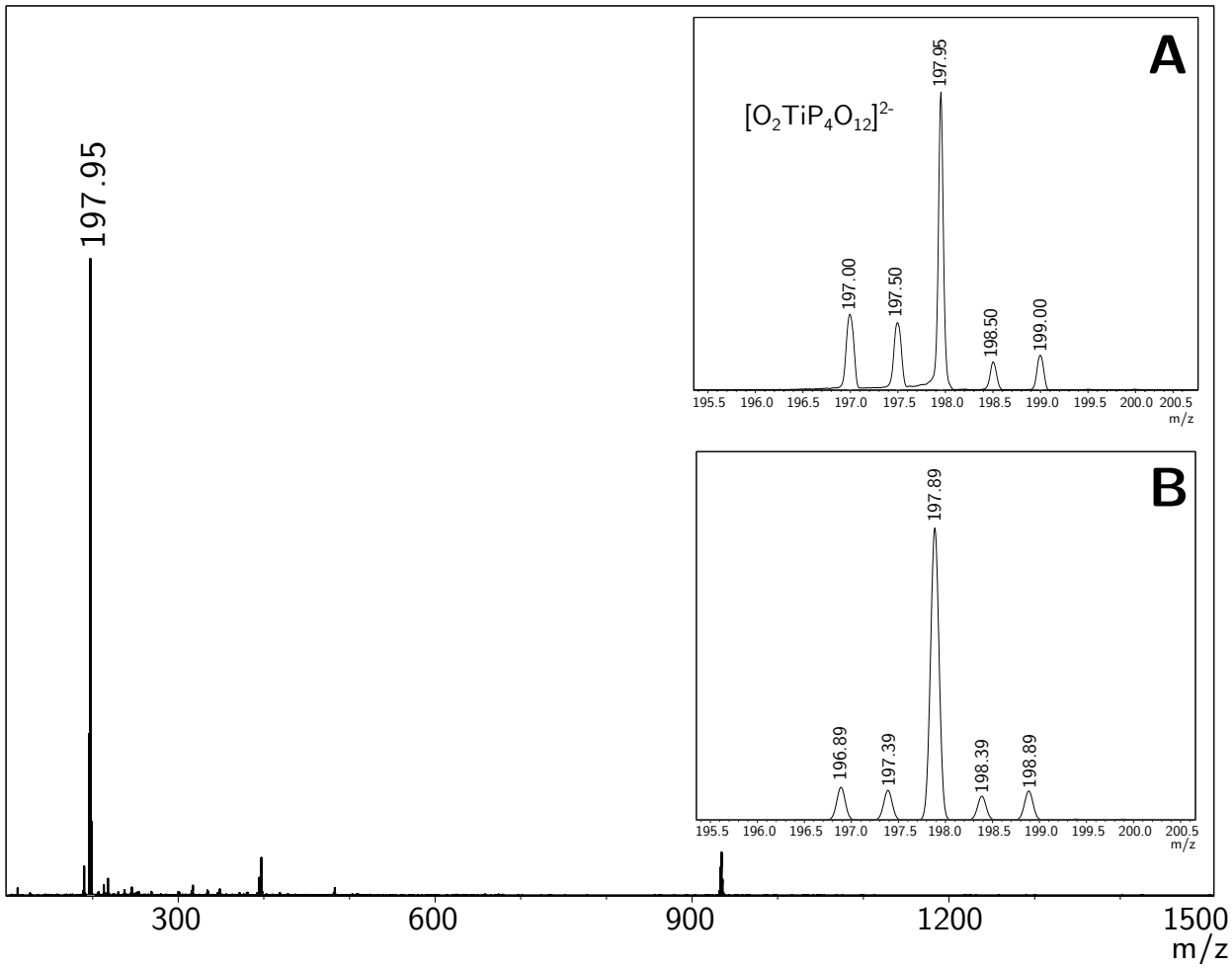

Figure S21: ESI-MS(–) of $[PPN]_4$[**3**]. **A**: Zoomed-in spectrum; **B**: simulated spectrum (MeCN, 3200 V).

1.4 [PPN]$_2$[$O_2TiP_3O_9$(acac)] ([PPN]$_2$[4]).

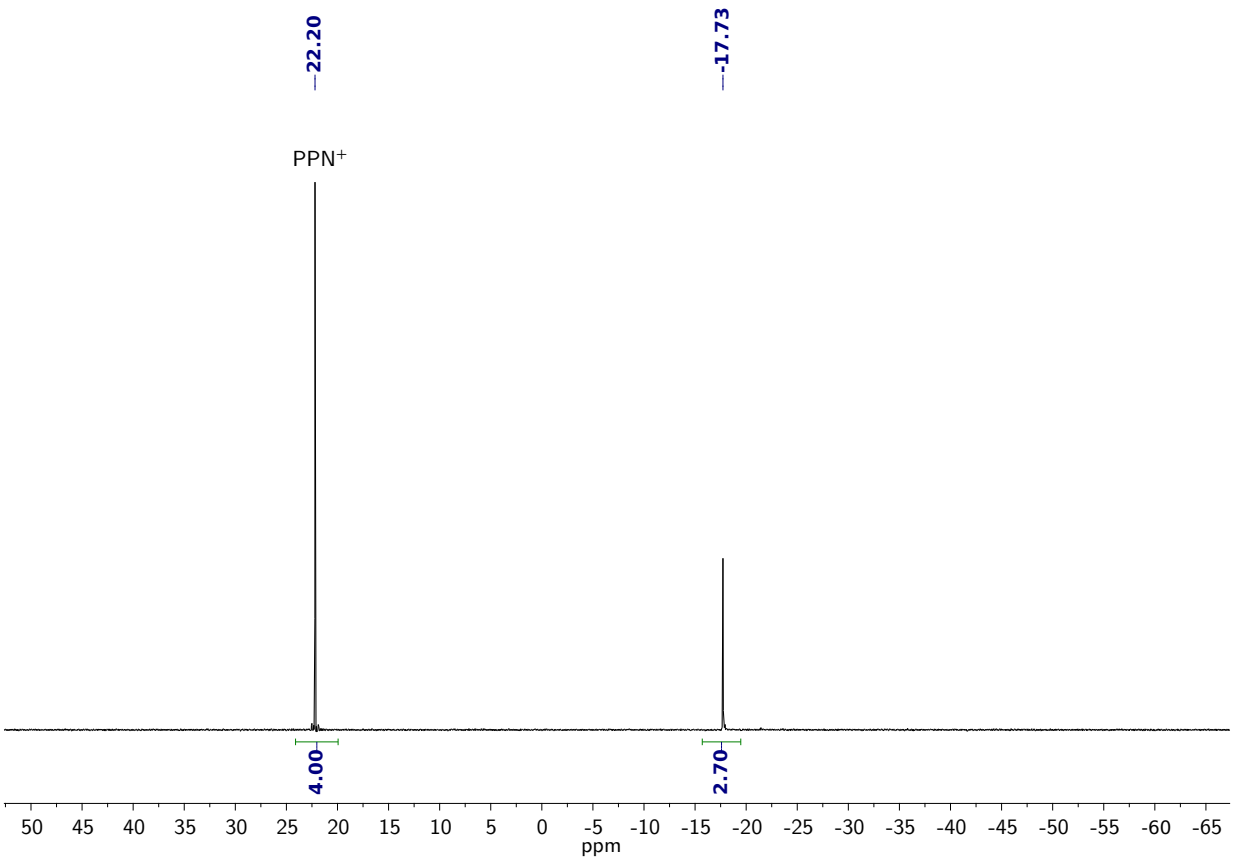

Figure S22: $^{31}P\{^1H\}$ NMR spectrum of [PPN]$_2$[**4**] (CD_3CN, 162 MHz, 25 °C).

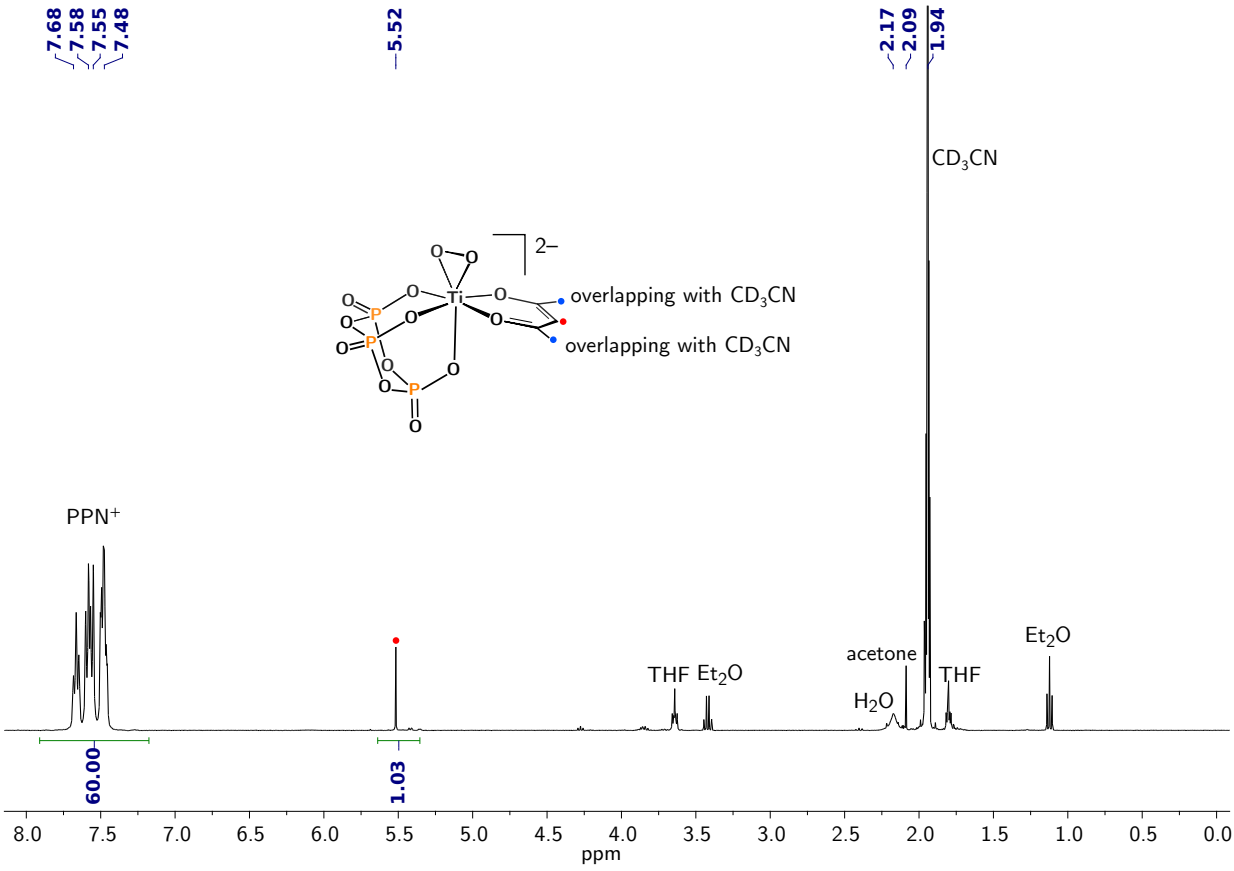

Figure S23: ^{1}H NMR spectrum of [PPN]$_2$[**4**] (CD_3CN, 400.1 MHz, 25 °C).

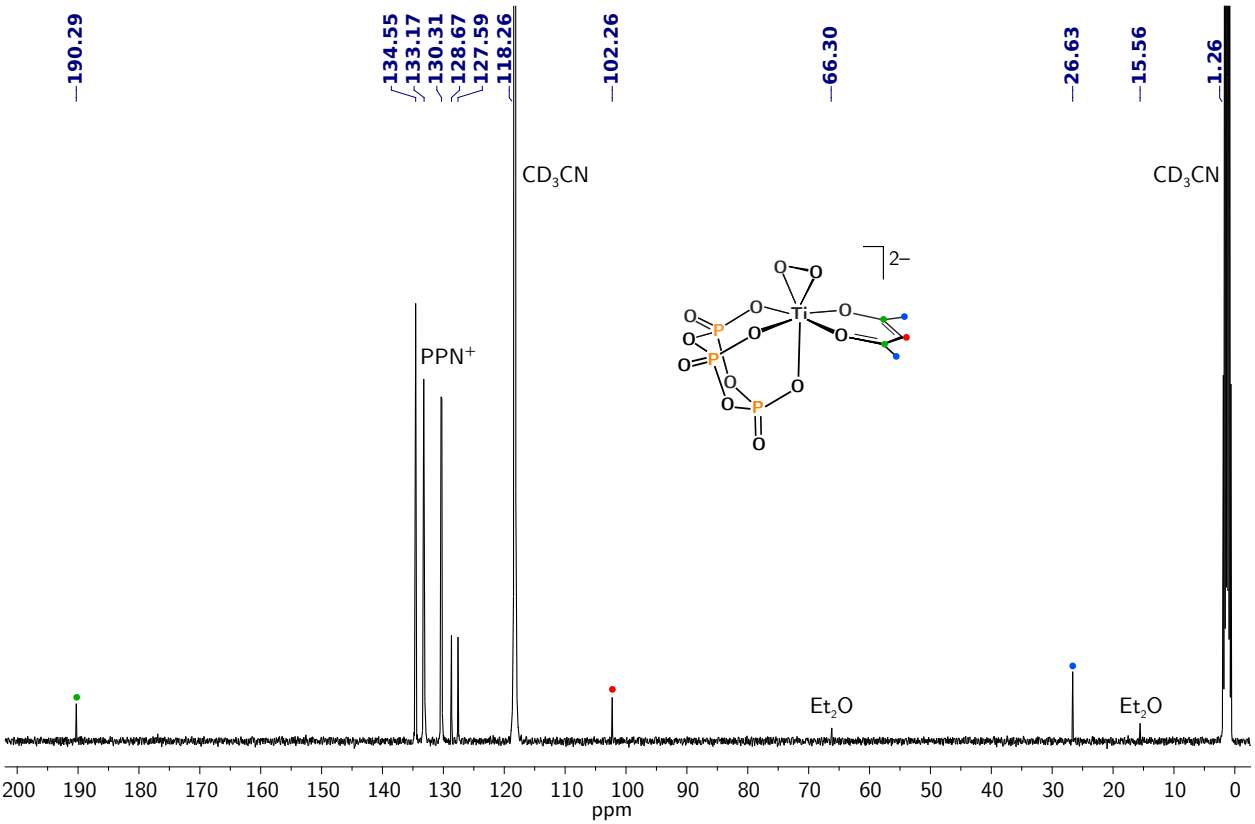

Figure S24: $^{13}C\{^{1}H\}$ NMR spectrum of $[PPN]_2$[**4**] (CD_3CN, 101 MHz, 25 °C).

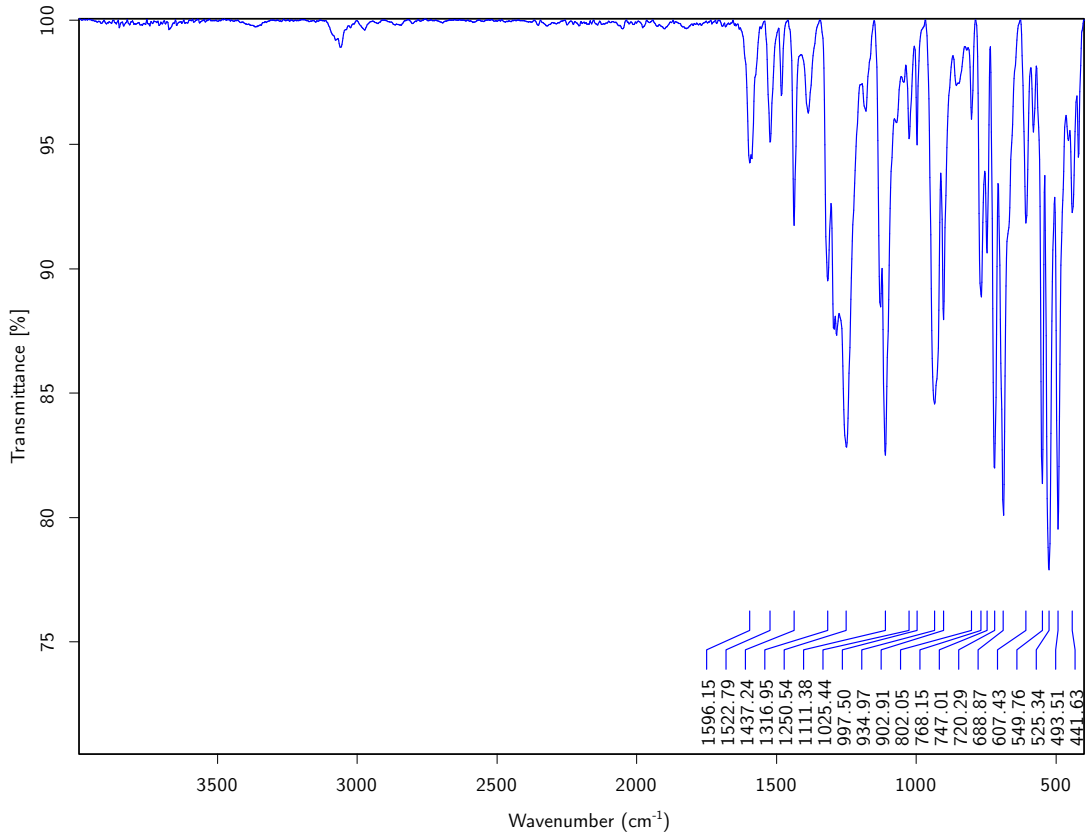

Figure S25: ATR-IR of $[PPN]_2$[**4**].

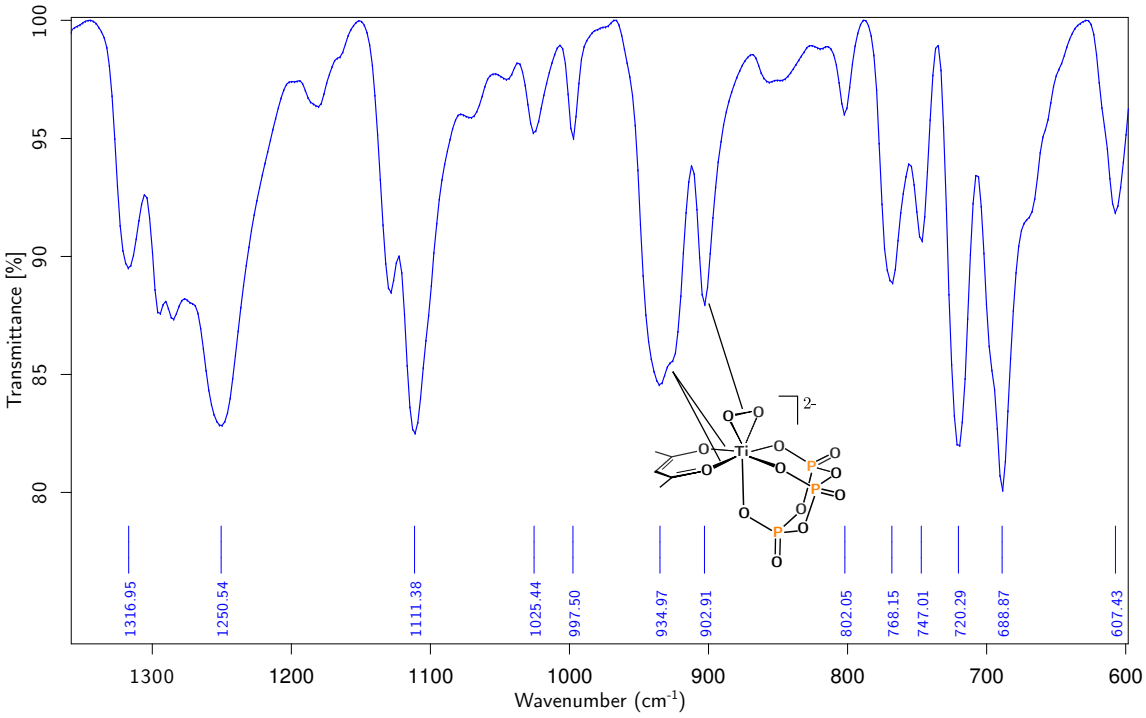

Figure S26: Zoomed-in ATR-IR of $[PPN]_2$[**4**].

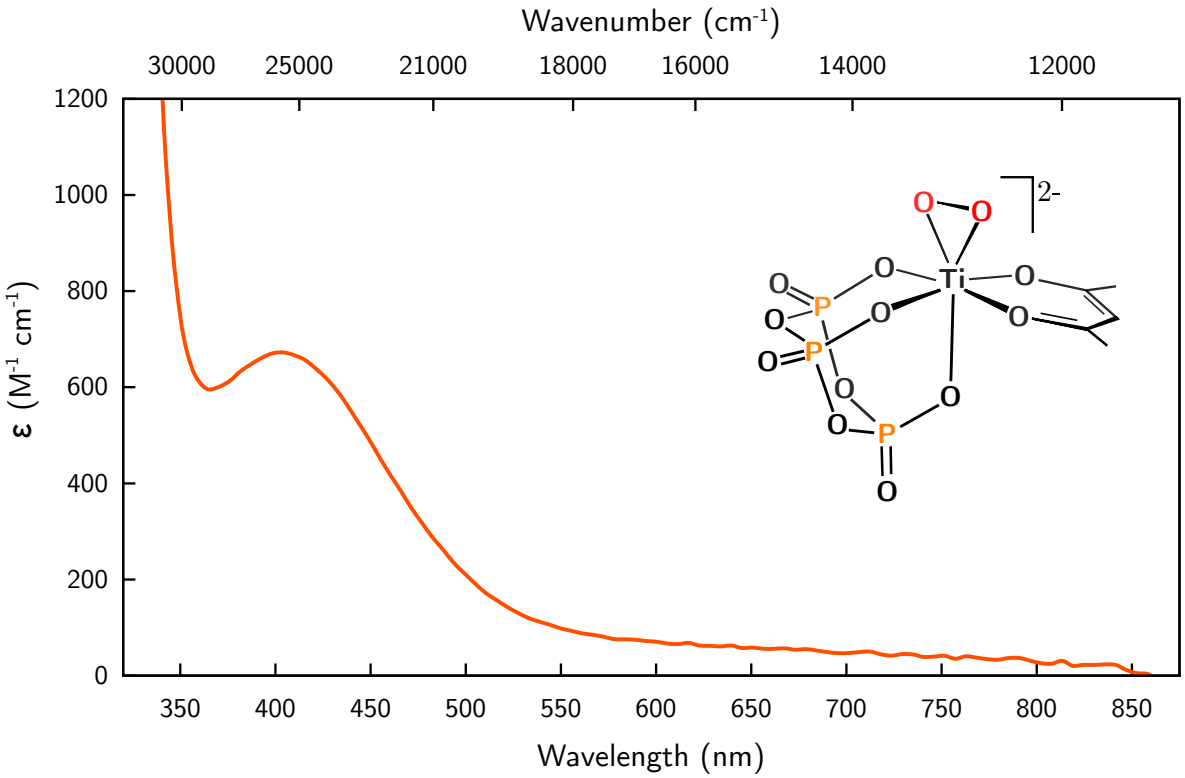

Figure S27: UV-Vis spectrum of $[PPN]_2$[**4**] (1.0 mM, MeCN, 20 °C).

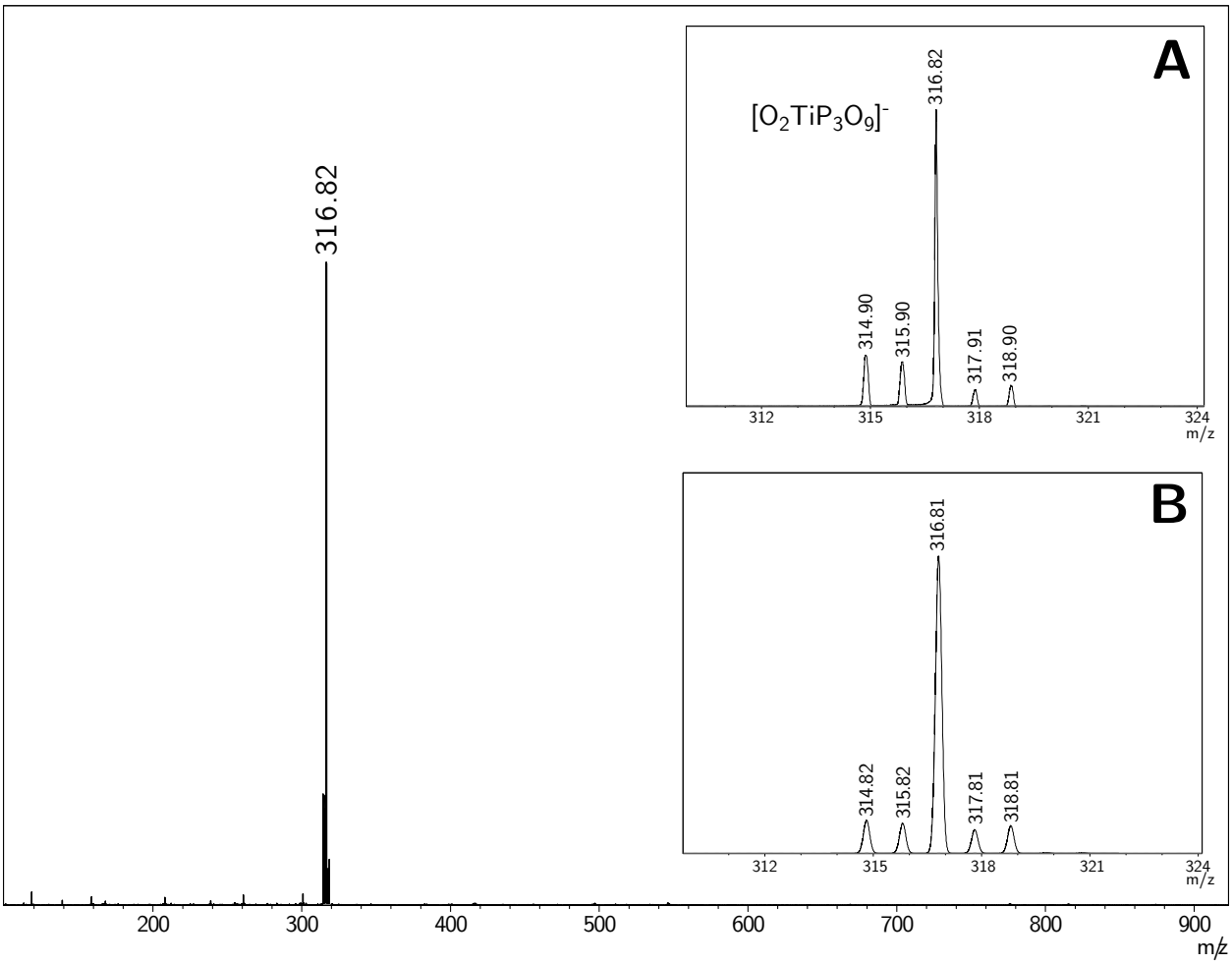

Figure S28: ESI-MS(–) of $[PPN]_2$[**4**]. **A**: Zoomed-in spectrum; **B**: simulated spectrum (MeCN, 3200 V). The acac ligand is not observable under ESI-MS(–) conditions.

2 Variable Temperature $^{31}P\{^{1}H\}$ NMR spectra of $[PPN]_2$[2].

A solution of $[PPN]_2$[**2**] (10 mg) was prepared in MeCN (0.5 mL). An initial $^{31}P\{^{1}H\}$ NMR spectrum of the sample was collected (25 °C), and then the temperature of the NMR probe was cooled in increments of 10 °C until a final temperature of –35 °C was reached. $^{31}P\{^{1}H\}$ NMR spectra were collected every 10 °C, and the temperatures were calibrated with methods reported by Merbach et al. [1]

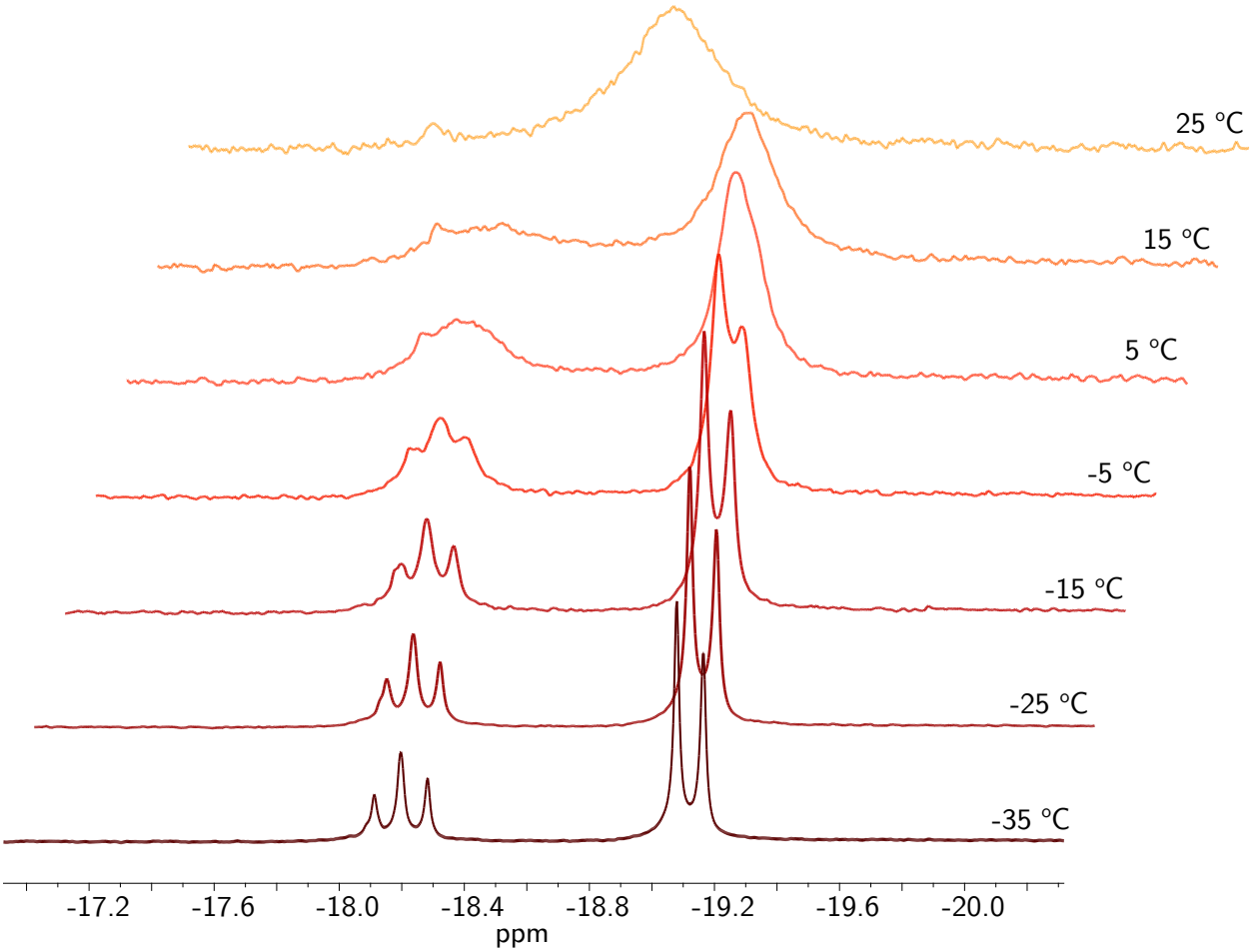

Figure S29: Variable temperature $^{31}P\{^{1}H\}$ NMR spectra of $[PPN]_2$[**2**] collected between 25 and –35 °C (MeCN, 202.4 MHz).

3 Evaluating the water stability of $[PPN]_2$[2].

A colorless solution of $[PPN]_2$[**2**] (10 mg, 0.0068 mmol, 1.0 eq) was prepared in MeCN (0.5 mL) and transferred to an NMR tube. To this solution was added H_2O (10 μL, 0.55 mmol, 82 eq) via 10 μL syringe, and a $^{31}P\{^1H\}$ NMR spectrum was immediately collected. To the same sample was added an additional 10 μL H_2O (20 μL total, 0.11 mmol total, 160 eq), and a $^{31}P\{^1H\}$ NMR spectrum was immediately collected, and then collected again after 24 h (Figure S30). There were no changes observed in the $^{31}P\{^1H\}$ NMR spectra after the H_2O additions.

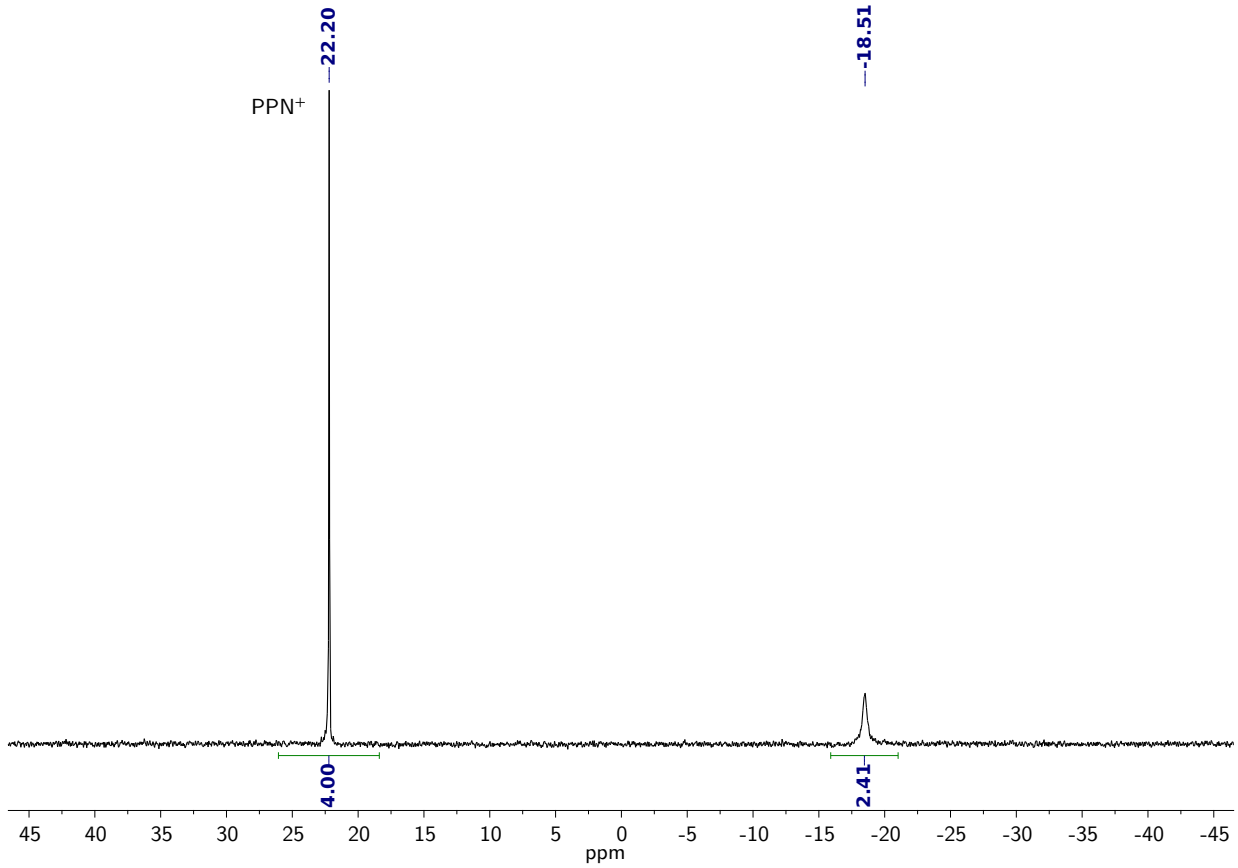

Figure S30: $^{31}P\{^1H\}$ NMR spectrum of a sample of $[PPN]_2$[**2**] in the presence of 160 eq H_2O after 24 h (MeCN, 162 MHz, 25 °C).

4 ^{17}O solution NMR spectrum of $[PPN]_2$[2].

A colorless solution of $[PPN]_2$[**2**] (15 mg, 0.010 mmol, 1.0 eq) was prepared in MeCN (0.5 mL) and transferred to an NMR tube. To this solution was added 70% $^{17}OH_2$ (10 μL, 0.55 mmol, 55 eq). The tube was capped and inverted to effect good mixing. A ^{17}O NMR spectrum (Figure S31) of this mixture was collected at 25 °C. After the acquisition was complete, a $^{31}P\{^1H\}$ NMR spectrum was collected, indicating the $[PPN]_2[OTiP_3O_9(acac)]$ complex remained intact in the presence of excess water during the course of the ^{17}O NMR experiment.

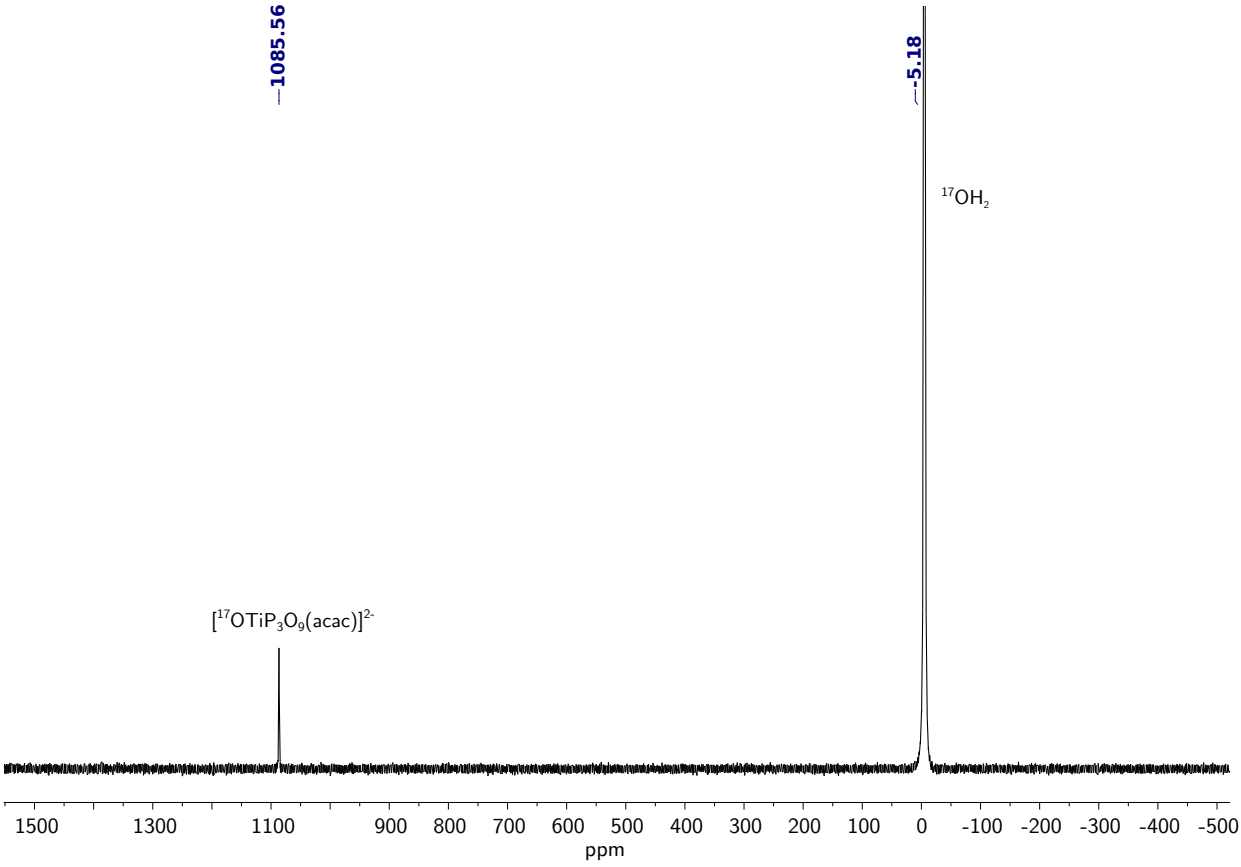

Figure S31: ^{17}O NMR spectrum of $[PPN]_2$[**2**] spiked with 70% $^{17}OH_2$ (10 μL, 55 eq). Externally referenced to D_2O (68 MHz, MeCN, 25 °C).

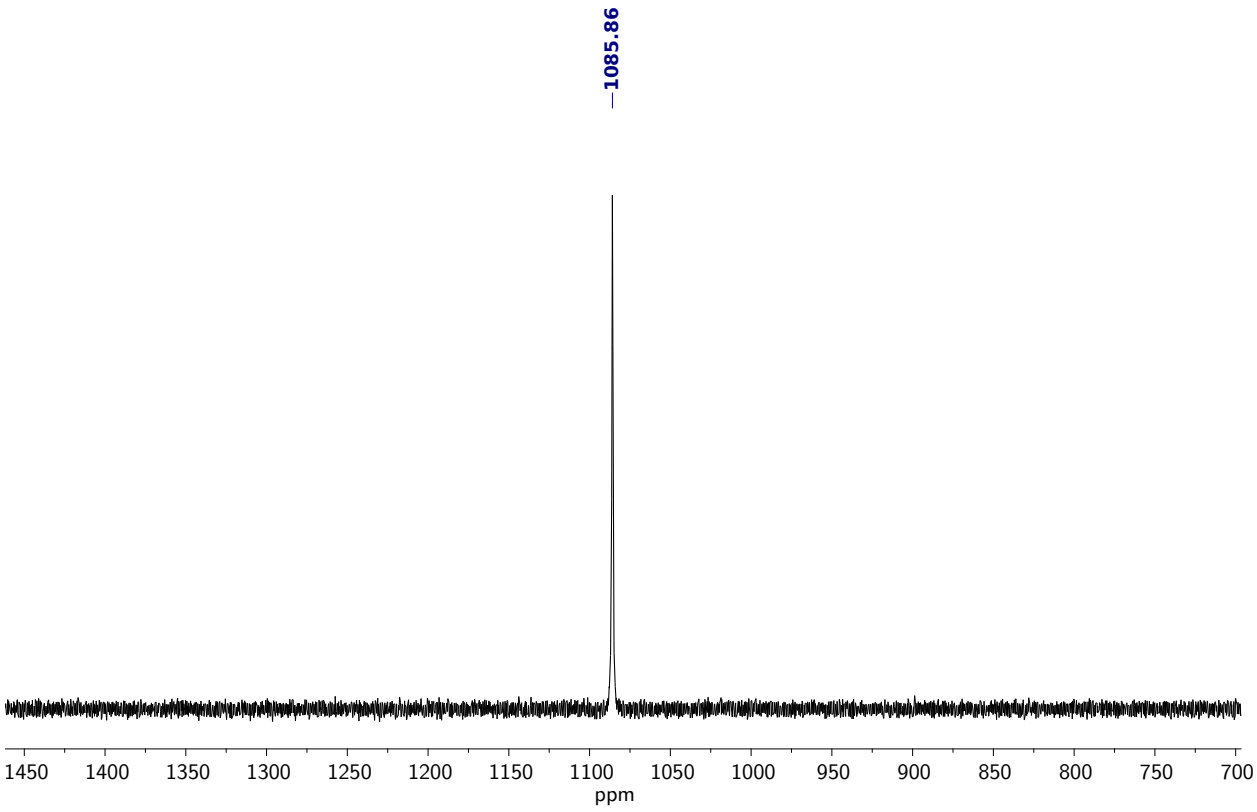

Figure S32: Zoomed-in ^{17}O NMR spectrum of $[PPN]_2$[**2**] spiked with 70% $^{17}OH_2$ (10 μL, 55 eq). Externally referenced to D_2O (68 MHz, MeCN, 25 °C).

5 Monitoring the conversion of $[PPN]_4[1]$ to $[PPN]_4[3]$ by UV-Vis spectroscopy.

A 1.0 mM solution of $[PPN]_4[OTiP_4O_{12}]_2$ was prepared in acetonitrile (2 mL) and transferred to a 1 cm path length Quartz cuvette. An initial UV-Vis spectrum was acquired, and then to this colorless solution was added urea hydrogen peroxide (2 mg, 0.06 mmol, 30 eq) as a solid. The cuvette was shaken to effect good mixing, and UV-Vis spectra were acquired every 60 sec for a total of 2 h.

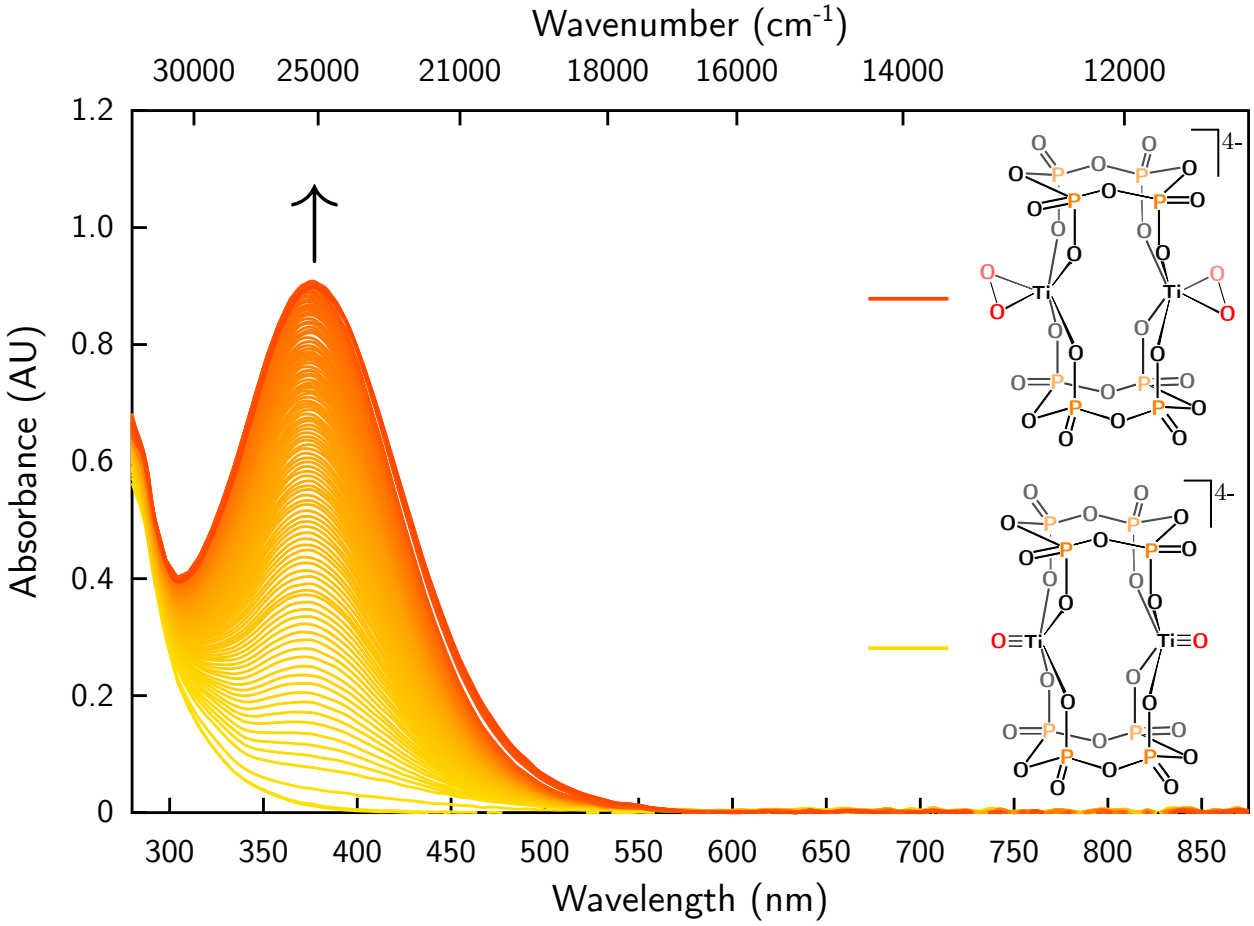

Figure S33: UV-Vis spectra displaying the conversion of $[PPN]_4$[**1**] to $[PPN]_4$[**3**] monitored over the course of 2 h (25 °C, MeCN, 1.0 mM).

6 Monitoring the conversion of $[PPN]_2$[2] to $[PPN]_2$[4] by UV-Vis spectroscopy.

A 1.0 mM solution of $[PPN]_2$[**2**] was prepared in acetonitrile (2 mL) and transferred to a 1 cm path length Quartz cuvette. An initial UV-Vis spectrum was acquired, and then to this colorless solution was added 30% aqueous hydrogen peroxide (2 μL, 0.1 mmol, 60 eq) via 10 μL syringe. UV-Vis spectra were acquired every 3 sec for a total of 10 min.

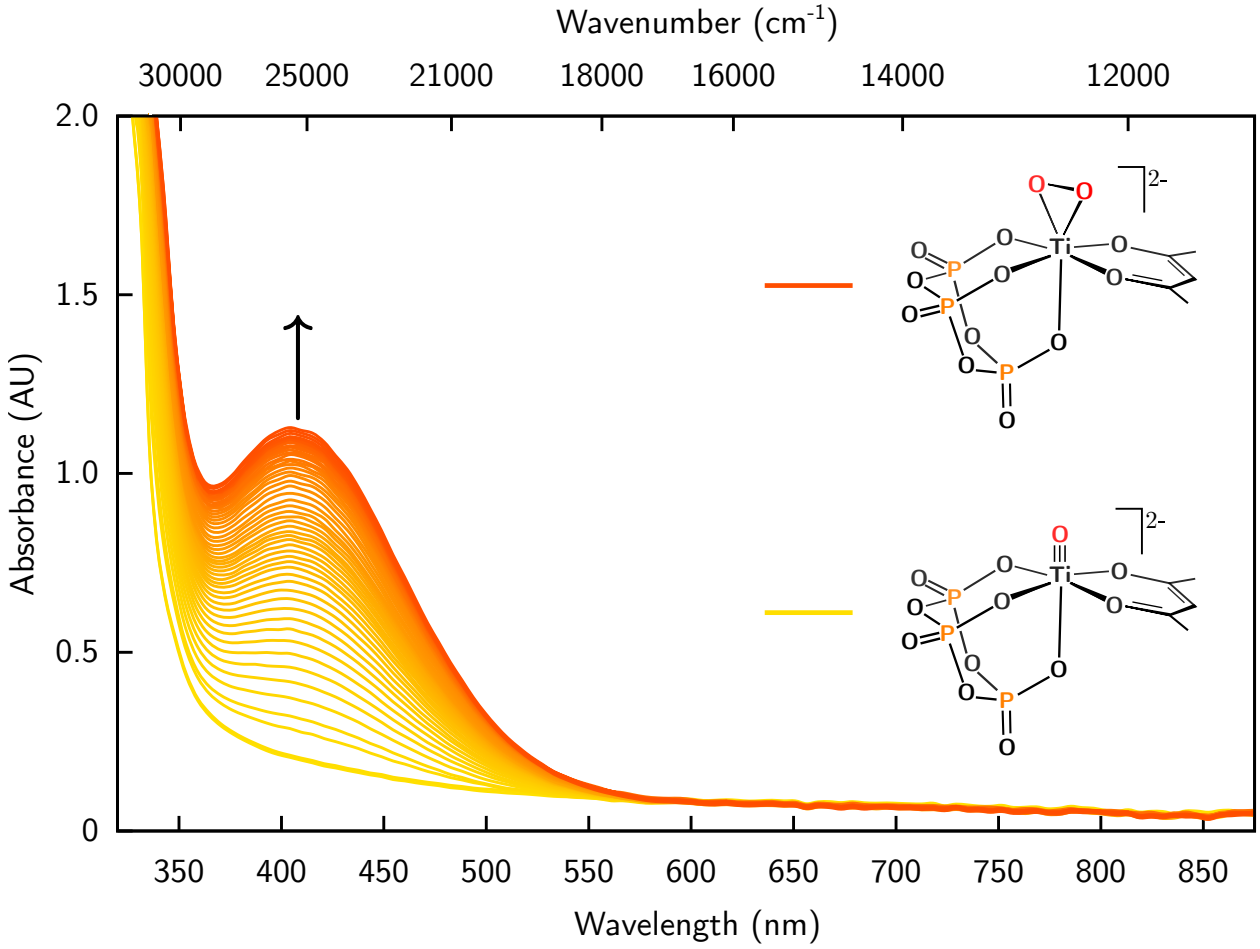

Figure S34: UV-Vis spectra of **2** upon treatment with 30% H_2O_2 collected every 3 sec over the course of 10 min (25 °C, 1.0 M, MeCN).

7 Monitoring the conversion of $[PPN]_4$[1] to $[PPN]_4$[3] by ^{31}P NMR spectroscopy at 5 °C.

A solution of $[PPN]_4$[**1**] (10 mg, 0.0034 mmol, 1.0 eq) was prepared in MeCN and transferred to an NMR tube. An initial $^{31}P\{^1H\}$ NMR spectrum was collected, and then the solution was frozen in a dry ice/acetone slush bath. While the solution was allowed to freeze, the NMR probe was cooled to 5 °C. Solid UHP (approx. 5 mg, 0.055 mmol, 16 eq) was then added on top of the frozen solution. The tube was capped, and then quickly inserted into the pre-cooled NMR probe. Spectra were collected every 4 min for a total of 76 min, and temperatures were calibrated with methods reported by Merbach et al.[1]

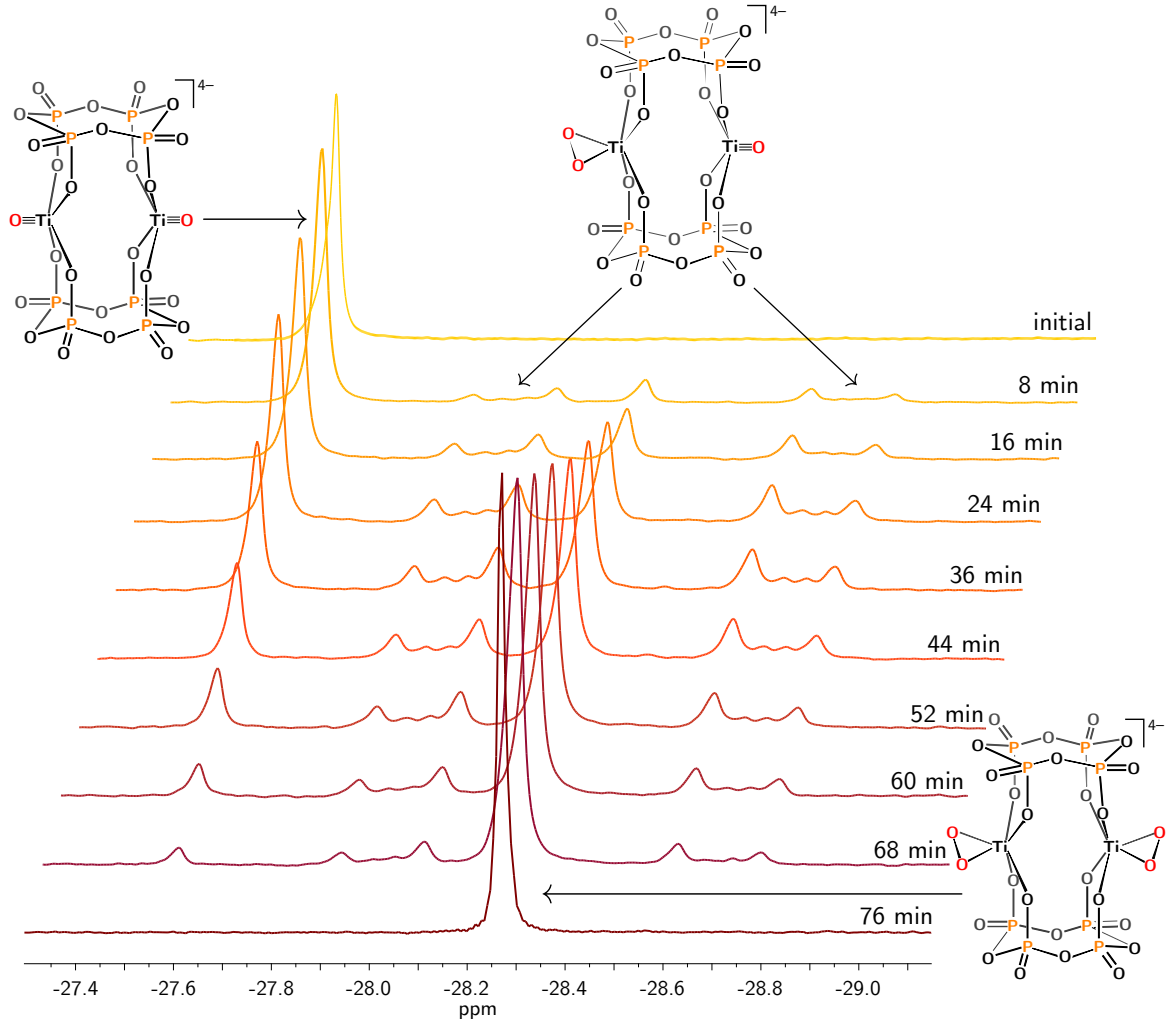

Figure S35: $^{31}P\{^1H\}$ NMR spectra of a solution of **1** treated with UHP monitored over the course of 76 min at 5 °C (MeCN, 202.4 MHz).

8 ESI-MS(–) data displaying exchange of the titanyl oxygen of $[PPN]_2$[2] with $^{18}OH_2$ and $^{17}OH_2$.

Two solutions of $[PPN]_2$[**2**] (<1 mg per sample) were prepared in MeCN (2 mL). $^{18}OH_2$ (97% enriched, 5 μL) was injected into one solution and $^{17}OH_2$ (70% enriched, 10 μL) was injected into the other solution via 10 μL syringe. ESI-MS (–) data for both solutions were immediately collected.

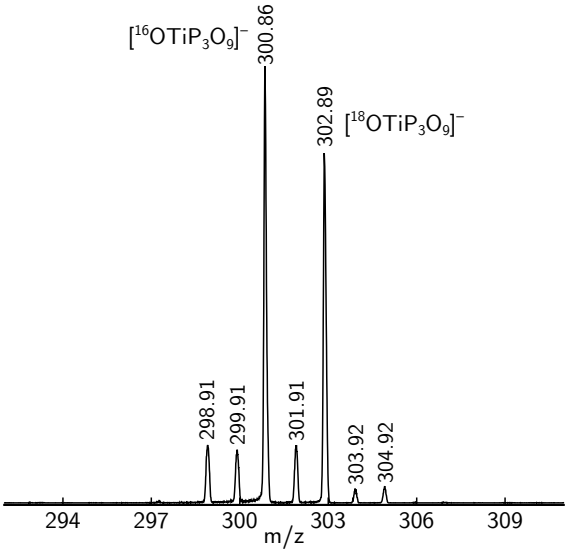

Figure S36: ESI-MS(–) of a sample of $[PPN]_2$[**2**] spiked with 5 μL of 97% enriched $^{18}OH_2$ (MeCN, 3200 V).

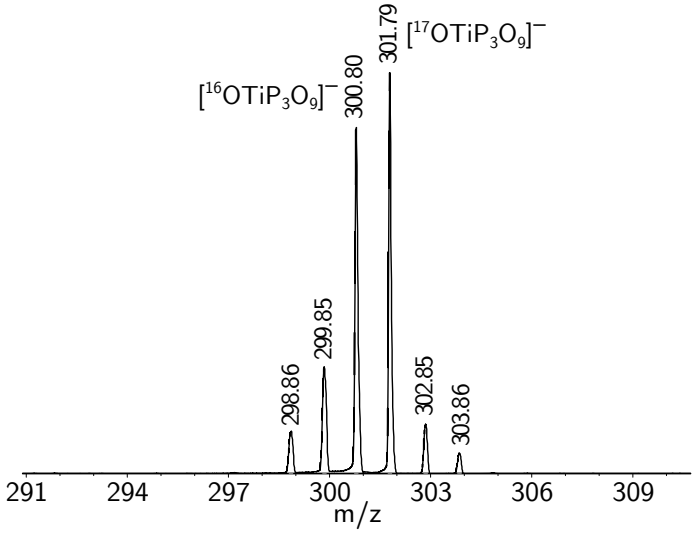

Figure S37: ESI-MS(–) of a sample of $[PPN]_2$[**2**] spiked with 10 μL of 70% enriched $^{17}OH_2$ (MeCN, 3200 V).

9 Treatment of $[PPN]_4[1]$ with $^{16}OH_2$ and $^{17}OH_2$.

9.1 $^{16}OH_2$.

To a colorless solution of $[PPN]_4$[**1**] (15 mg, 0.0050 mmol, 1.0 eq) in MeCN (0.5 mL) was added ACS reagent grade H_2O (10 μL, 0.52 mmol, 100 eq) via 10 μL syringe. A $^{31}P\{^1H\}$ NMR spectrum of this solution was immediately collected (Figure S38). The sample was allowed to stand at ambient temperature (22 °C) for an additional 24 h, at which point a $^{31}P\{^1H\}$ NMR spectrum was collected again (Figure S40).

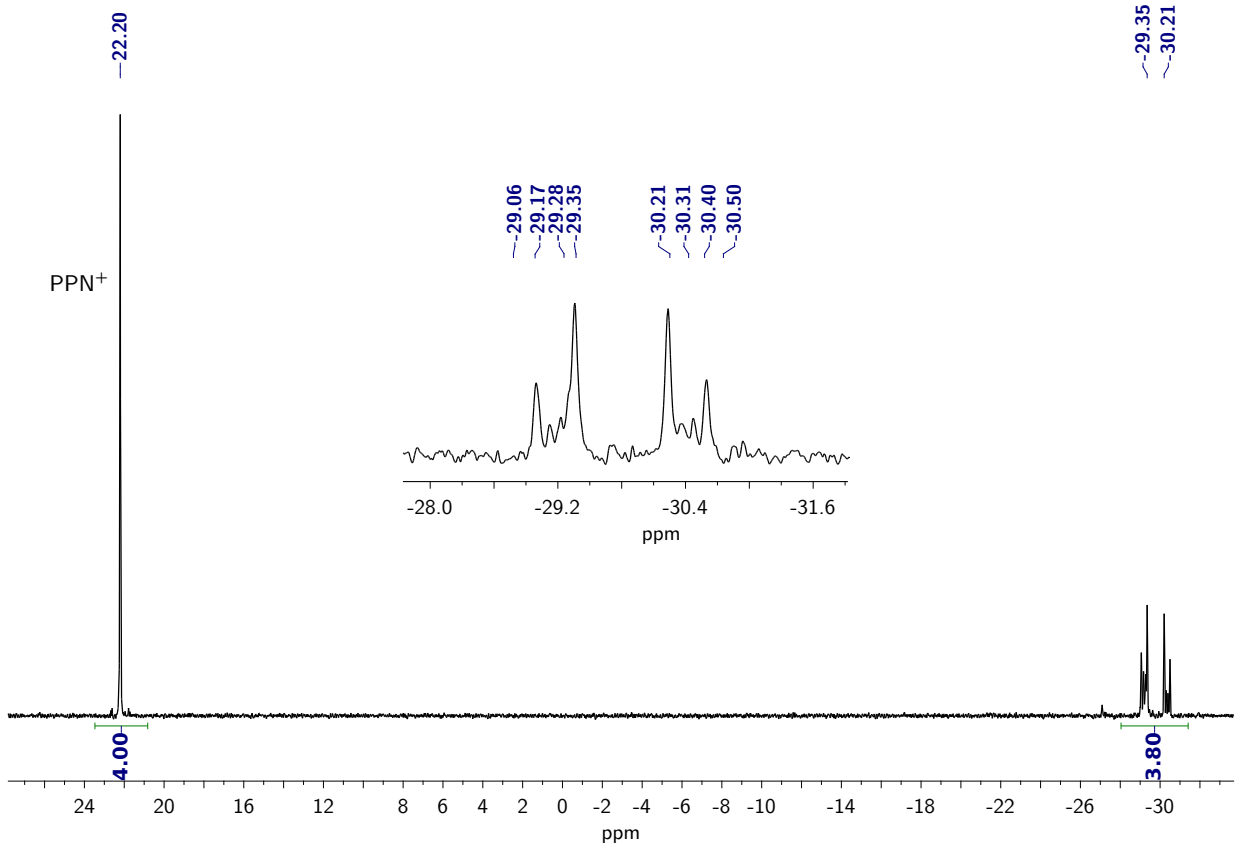

Figure S38: $^{31}P\{^1H\}$ NMR spectrum of $[PPN]_4$[**1**] after 10 min in the presence of 100 eq H_2O (MeCN, 162 MHz, 25 °C).

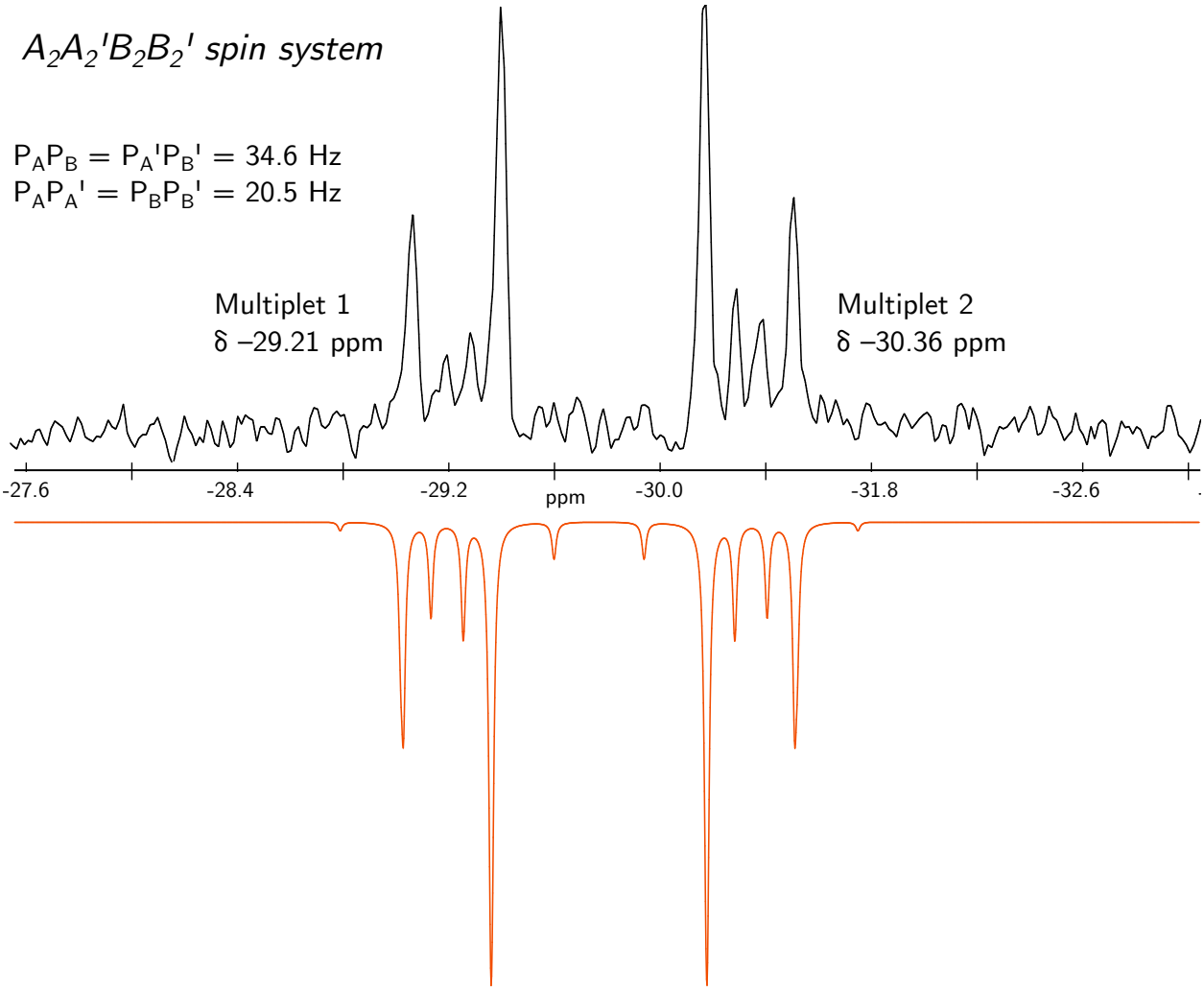

Figure S39: Top: $^{31}P\{^{1}H\}$ NMR spectrum of $[PPN]_4$[**1**] after 10 min in the presence of 100 eq H_2O (MeCN, 121.49 MHz, 25 °C). Bottom: ^{31}P NMR spectrum displaying an $A_2A_2'B_2B_2'$ splitting pattern[2] simulated using the program gNMR.[3]

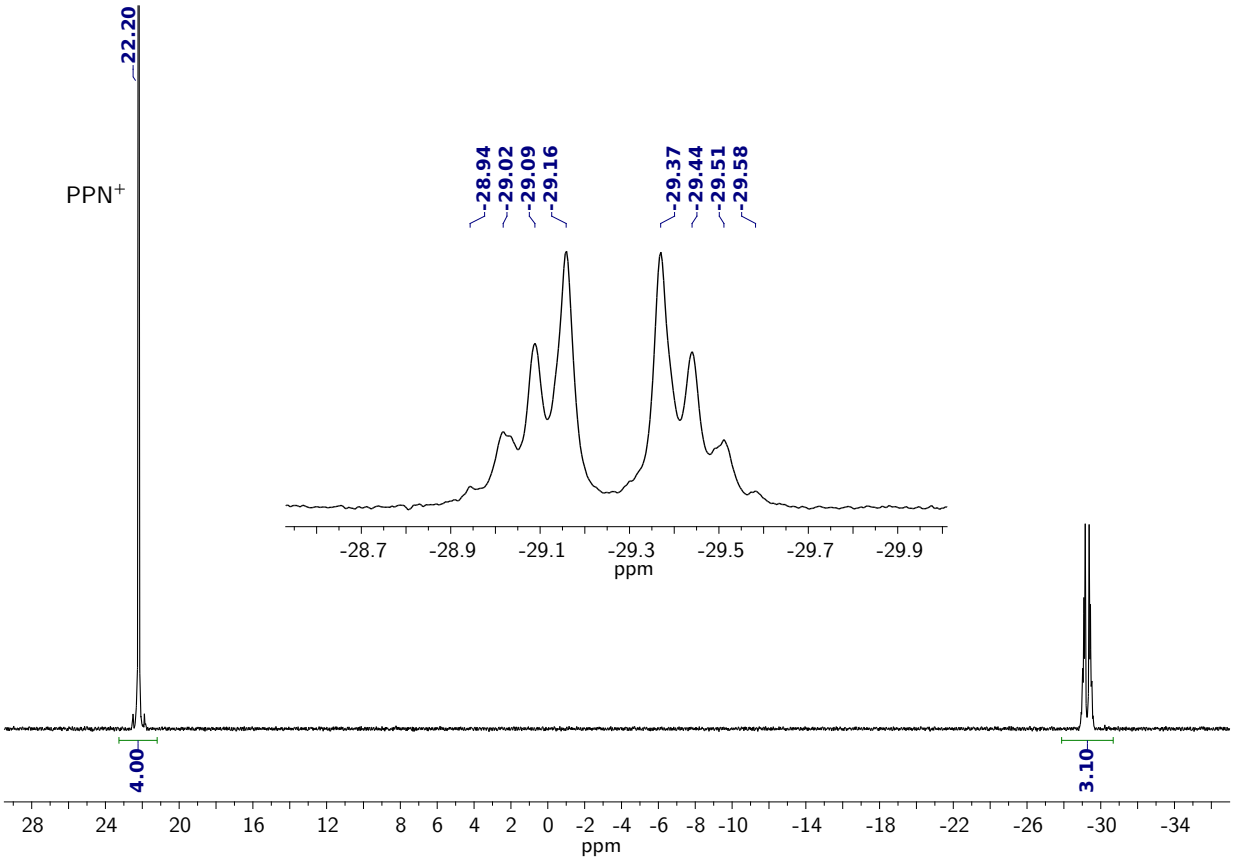

Figure S40: $^{31}P\{^{1}H\}$ NMR spectrum of $[PPN]_4$[**1**] after 24 h in the presence of 100 eq H_2O (MeCN, 162 MHz, 25 °C).

9.2 $^{17}OH_2$.

To a colorless solution of $[PPN]_4$[**1**] (15 mg, 0.0050 mmol, 1.0 eq) in MeCN (0.5 mL) was added 70% enriched $^{17}OH_2$ (5 μL, 0.3 mmol, 50 eq) via 10 μL syringe. ^{17}O and $^{31}P\{^1H\}$ NMR spectra of this solution were collected after 30 min (Figure S41). The sample was allowed to stand at ambient temperature (22 °C) for an additional 24 h, at which point ^{17}O and $^{31}P\{^1H\}$ NMR spectra were collected again (Figure S42).

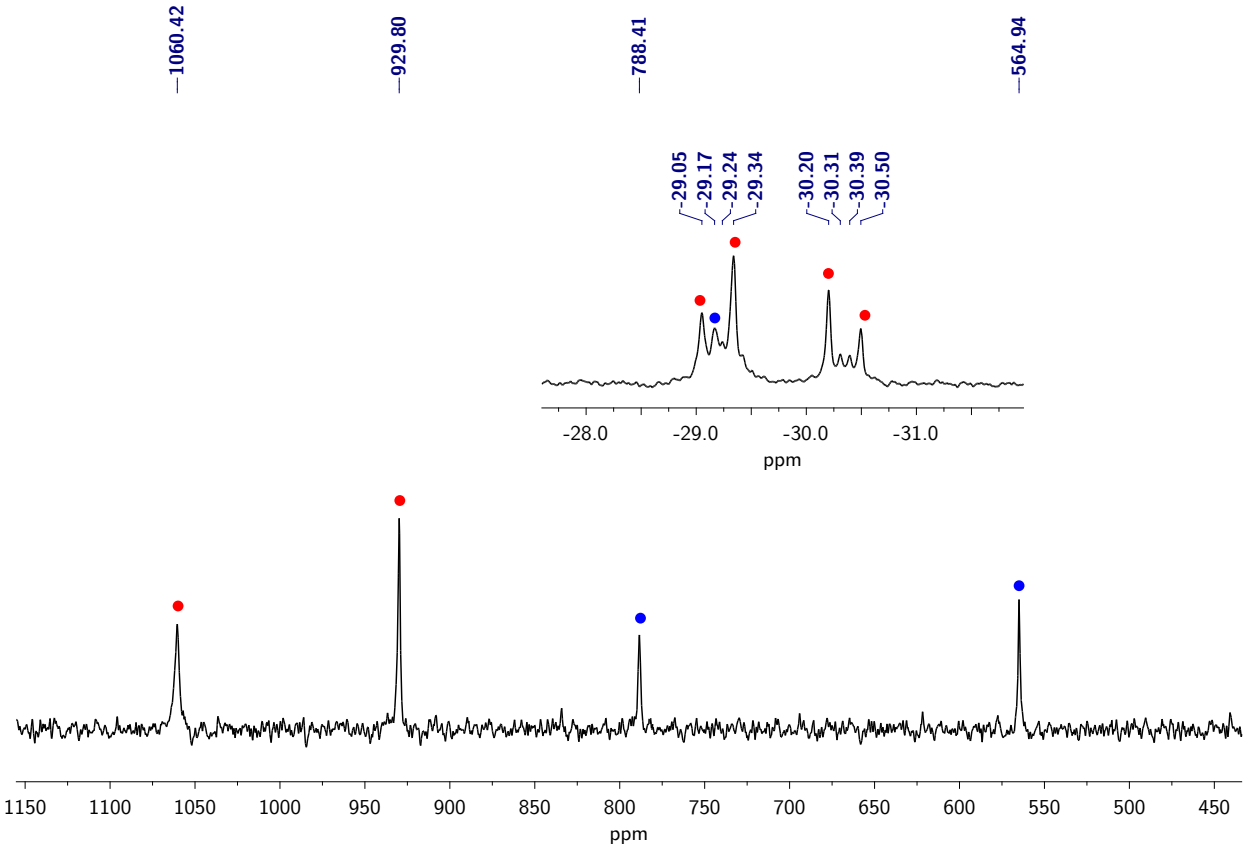

Figure S41: ^{17}O NMR spectrum of $[PPN]_4$[**1**] after 30 min in the presence of 50 eq $^{17}OH_2$ (externally referenced to D_2O, MeCN, 68 MHz, 25 °C). Inset: $^{31}P\{^1H\}$ NMR spectrum of the same solution (202.4 MHz).

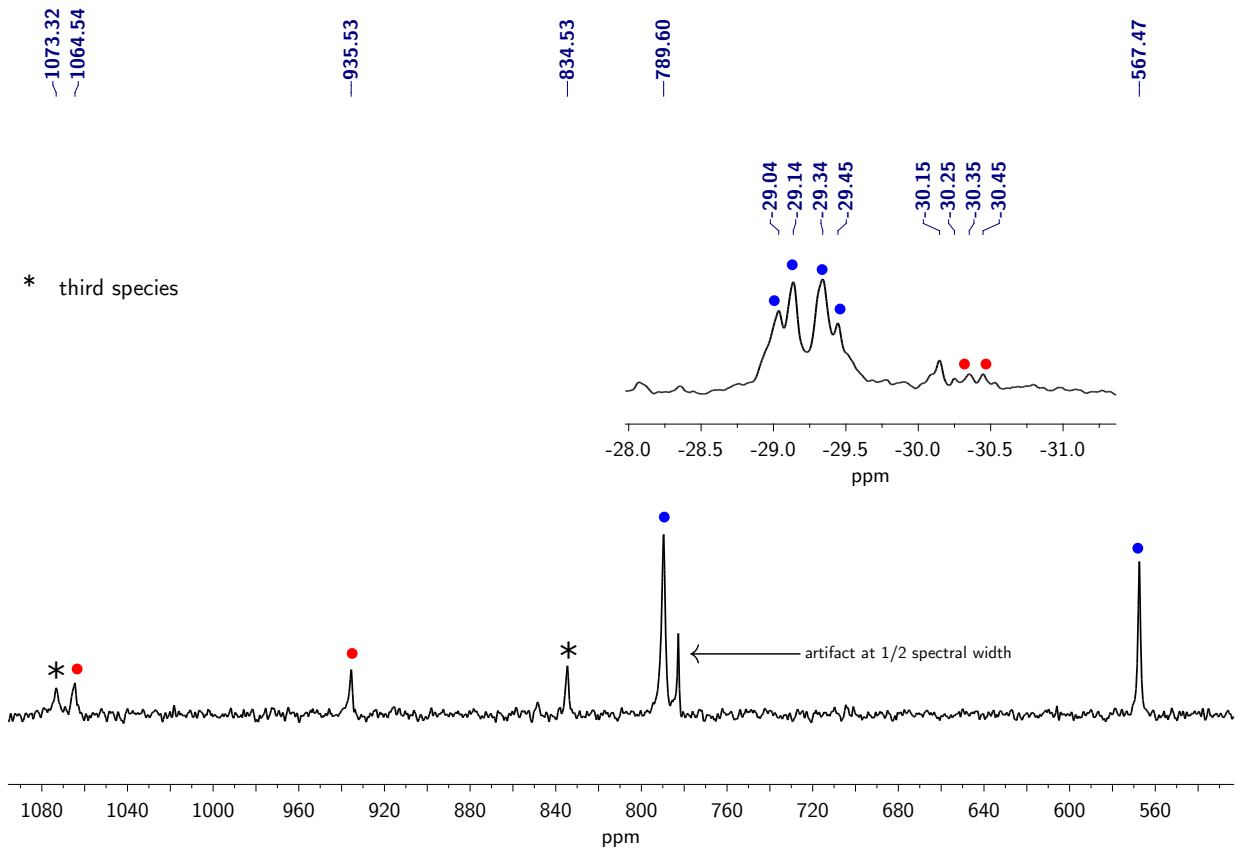

Figure S42: ^{17}O NMR spectrum of $[PPN]_4[\mathbf{1}]$ after 24 h in the presence of 50 eq $^{17}OH_2$ (externally referenced to D_2O, MeCN, 68 MHz, 25 °C). Inset: $^{31}P\{^1H\}$ NMR spectrum of the same solution (202.4 MHz).

10 Assessing the reversibility of the reaction of $[PPN]_4[1]$ with H_2O.

To a colorless solution of $[PPN]_4$[**1**] (15 mg, 0.0050 mmol, 1.0 eq) in MeCN (0.5 mL) was added ACS reagent grade H_2O (10 μL, 0.52 mmol, 100 eq) via 10 μL syringe. A $^{31}P\{^1H\}$ NMR spectrum of this solution was immediately collected (Figure S43, top). The contents of the NMR tube were then transferred to a 20 mL scintillation vial. The vial and its contents were heated at 80 °C under vacuum for 2 h. The colorless residue was then dissolved in MeCN (0.5 mL), and a $^{31}P\{^1H\}$ NMR spectrum (Figure S43, middle) of the resulting solution was collected. This procedure was repeated once more such that the sample was heated to 80 °C under vacuum for a total of 5 h, at which point a final $^{31}P\{^1H\}$ NMR spectrum (Figure S43, bottom) of the residue was collected in MeCN (0.5 mL).

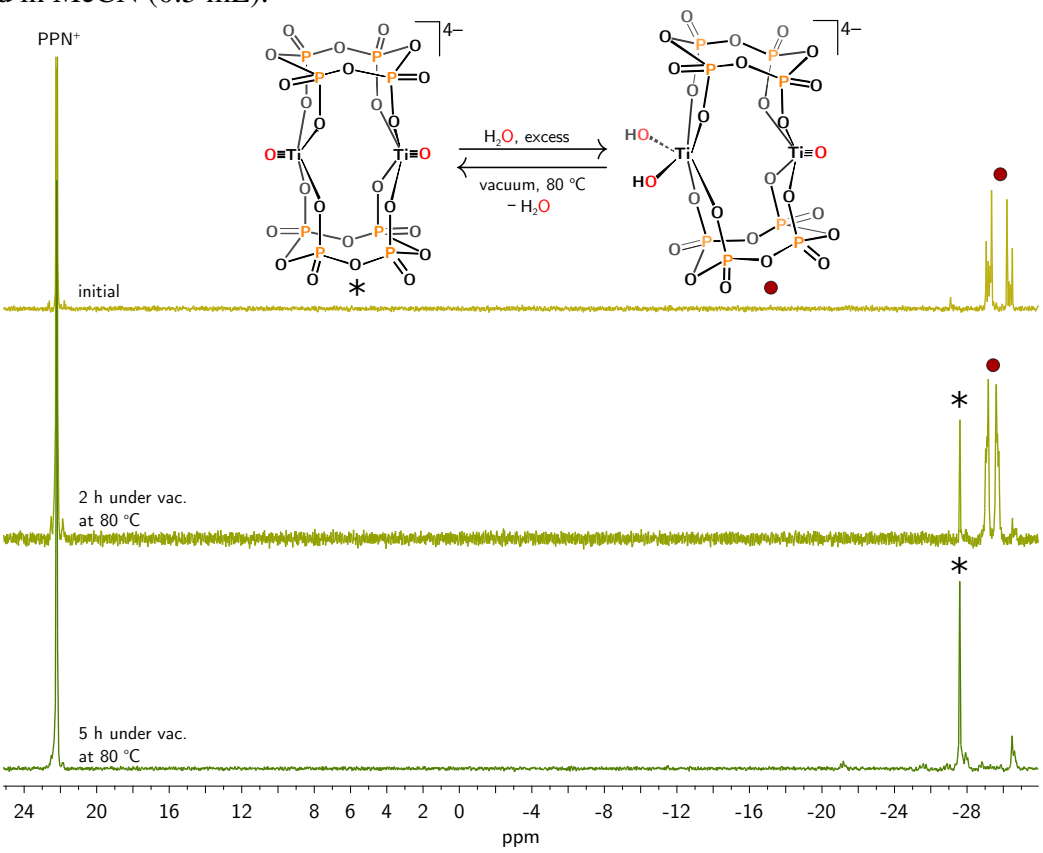

Figure S43: $^{31}P\{^1H\}$ NMR spectra of a solution of $[PPN]_4$[**1**] after initial treatment with 100 eq H_2O (top), after the solution was heated to 80 °C under vacuum for 2 h and redissolved in MeCN (middle), and after the solution was heated to 80 °C under vacuum for 5 h and redissolved in MeCN (bottom). MeCN, 121 MHz, 25 °C.

11 Oxygen atom transfer (OAT) from $[PPN]_4[3]$ to $P(OMe)_3$, PPh_3, and SMe_2.

11.1 $P(OMe)_3$.

To a MeCN (0.4 mL) solution of $[PPN]_4$[**3**] (10 mg, 0.0034 mmol, 1.0 eq) in an NMR tube was added neat $P(OMe)_3$ (4 μL, 0.034 mmol, 10 eq) via 10 μL syringe. A $^{31}P\{^1H\}$ NMR spectrum of the reaction mixture was collected after 10 min.

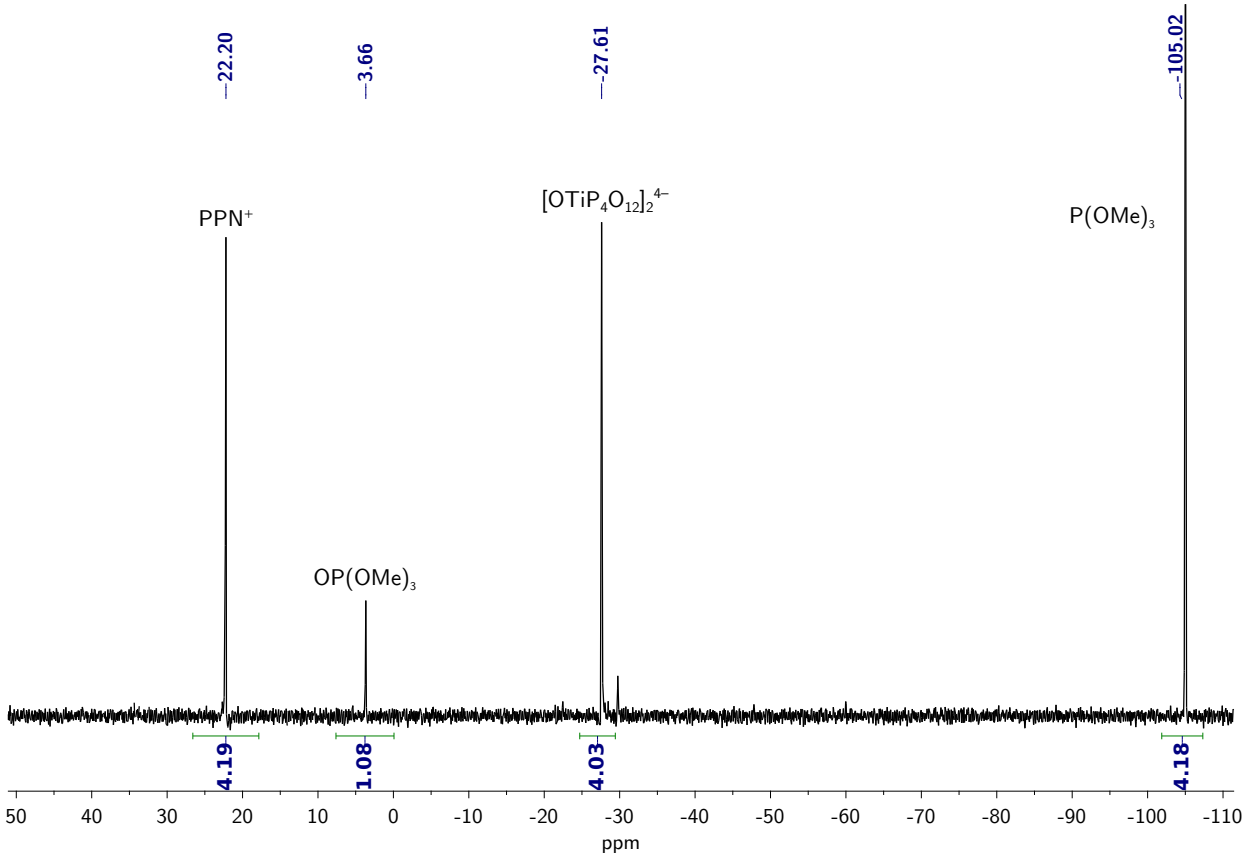

Figure S44: $^{31}P\{^1H\}$ NMR spectra of a solution of $[PPN]_4$[**3**] after treatment with 10 eq $P(OMe)_3$ at 23 °C after 10 min (MeCN, 121 MHz, 25 °C).

11.2 PPh_3.

To a MeCN (0.4 mL) solution of $[PPN]_4$[**3**] (10 mg, 0.0034 mmol, 1.0 eq) in an NMR tube was added a solution of PPh_3 (4 mg, 0.01 mmol, 4 eq) in MeCN (0.1 mL). A $^{31}P\{^1H\}$ NMR spectrum was collected immediately (Figure S45, top), and then again after 30 min (Figure S45, bottom).

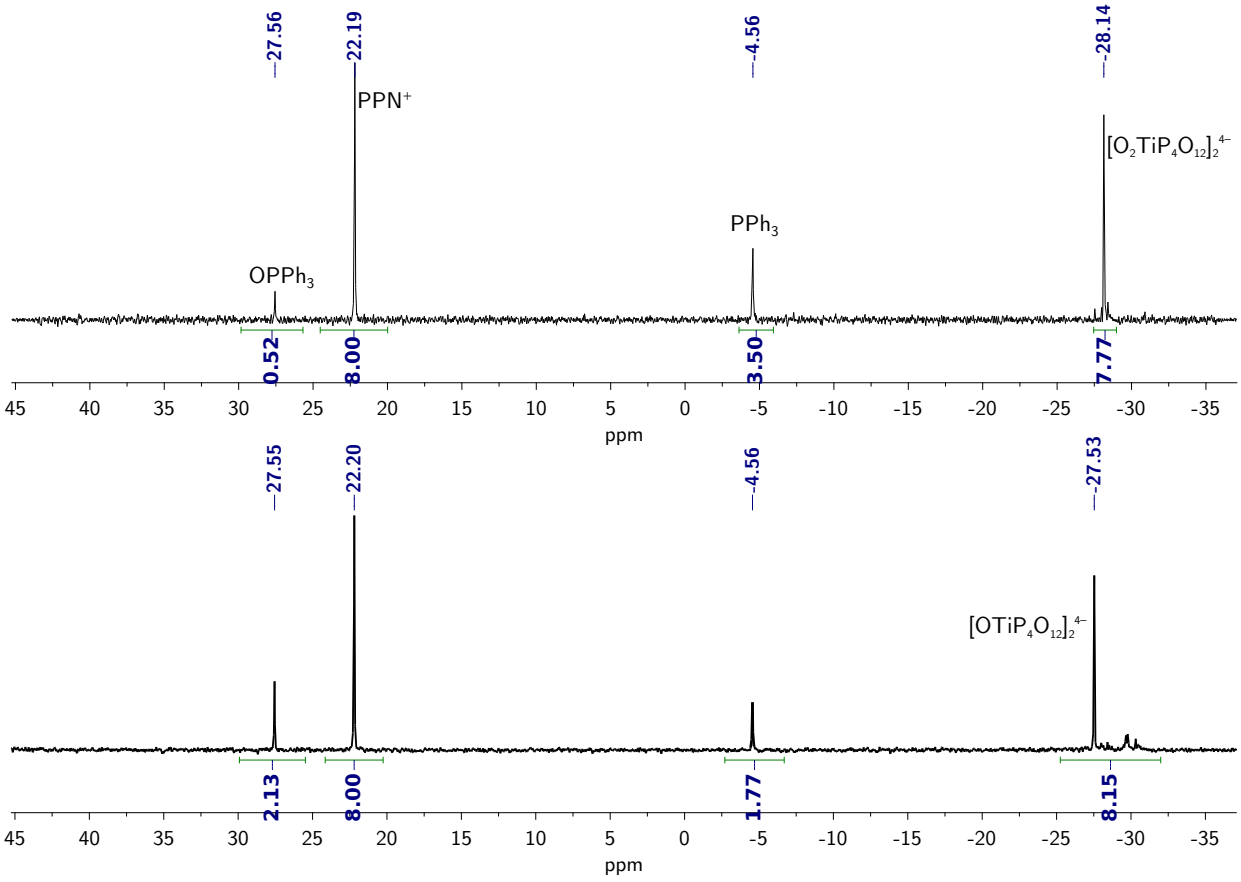

Figure S45: $^{31}P\{^1H\}$ NMR spectra of a solution of $[PPN]_4$[**3**] after treatment with 4 eq PPh_3 at 23 °C after 30 sec (top), and after 30 min (bottom). MeCN, 121 MHz, 25 °C.

11.3 SMe_2.

To a solution of $[PPN]_4$[**3**] (10 mg, 0.0034 mmol, 1.0 eq) in CD_3CN (0.5 mL) was added SMe_2 (2 μL, 0.03 mmol, 10 eq) via 10 μL syringe. ^1H (Figure S46) and $^{31}P\{^1H\}$ NMR (Figure S47) spectra were collected after 2 h of reaction time at 23 °C.

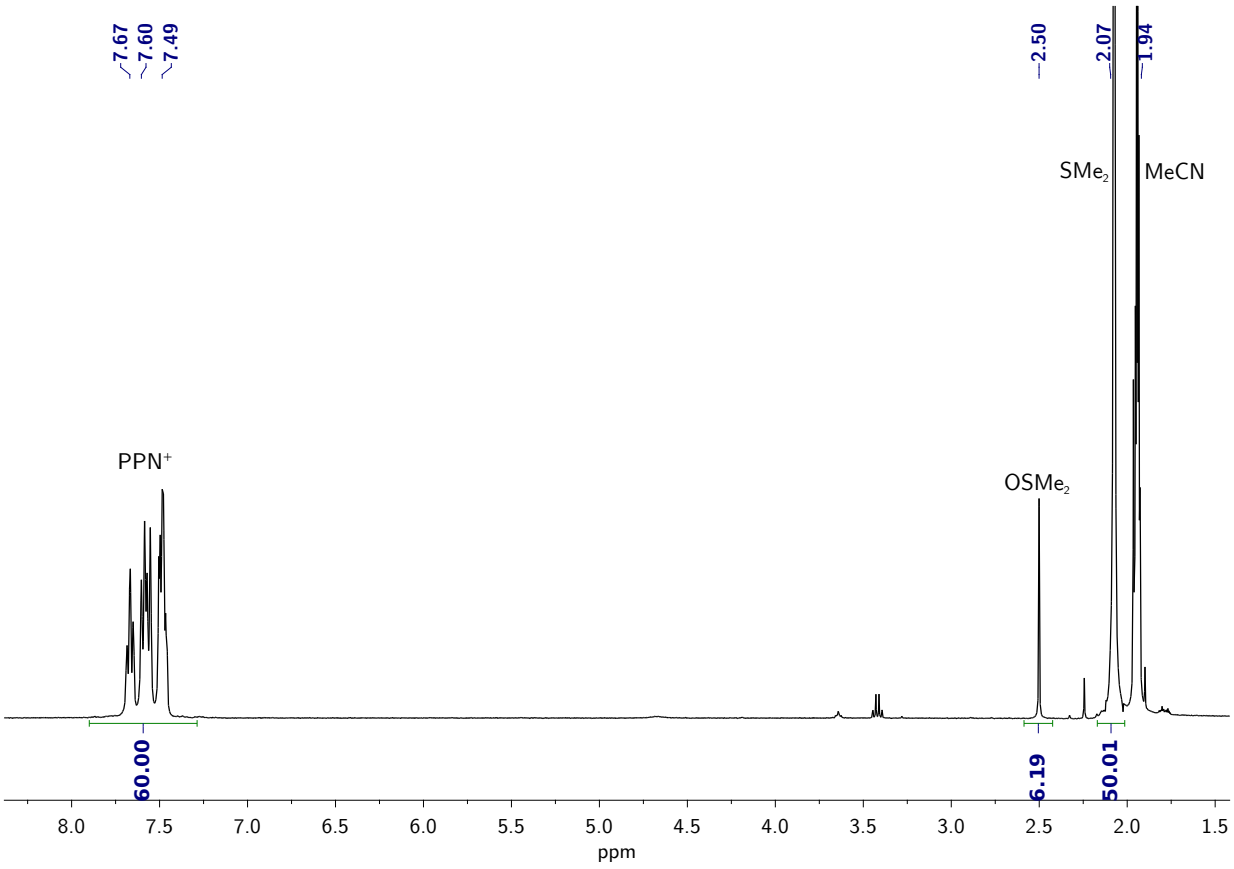

Figure S46: ^1H NMR spectrum of a solution of $[PPN]_4$[**3**] after treatment with 10 eq SMe_2 at 23 °C after 2 h (CD_3CN, 400 MHz, 25 °C).

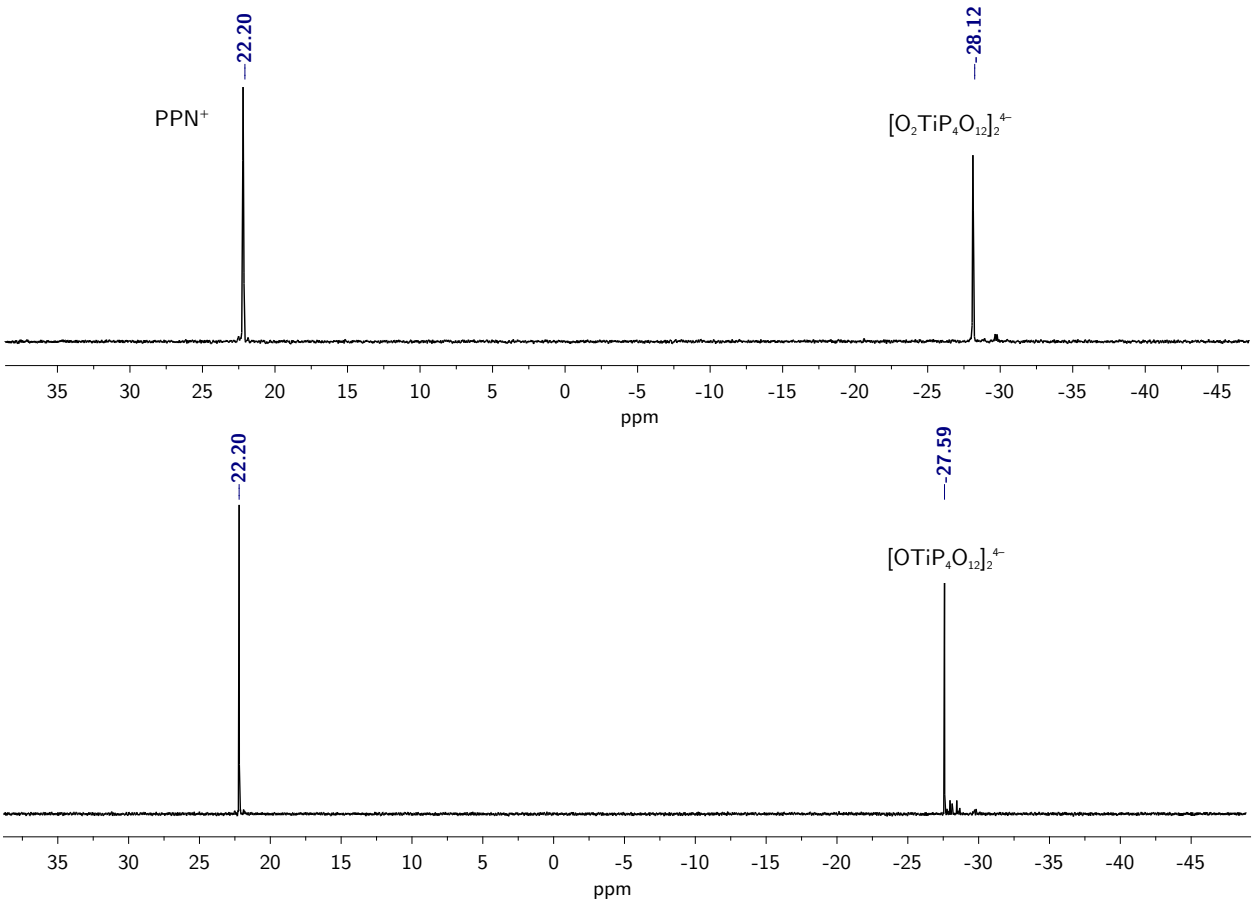

Figure S47: Initial $^{31}P\{^{1}H\}$ NMR spectra of a solution of $[PPN]_4$[**3**] (top), and 2 h after treatment with 10 eq SMe_2 at 23 °C (bottom) (CD_3CN, 400 MHz, 25 °C).

12 Oxygen atom transfer (OAT) from $[PPN]_2$[4] to PPh_3.

To a MeCN (0.4 mL) solution of $[PPN]_4$[**4**] (15 mg, 0.010 mmol, 1.0 eq) in an NMR tube was added a solution of PPh_3 (4 mg, 0.02 mmol, 1.5 eq) in MeCN (0.1 mL). A $^{31}P\{^1H\}$ NMR spectrum was collected immediately (Figure S48, top), and then the tube was placed in a preheated oil bath set to 80 °C. A $^{31}P\{^1H\}$ NMR spectrum of the sample was collected again after the reaction had been heated for 1 h at 70 °C (Figure S48, bottom).

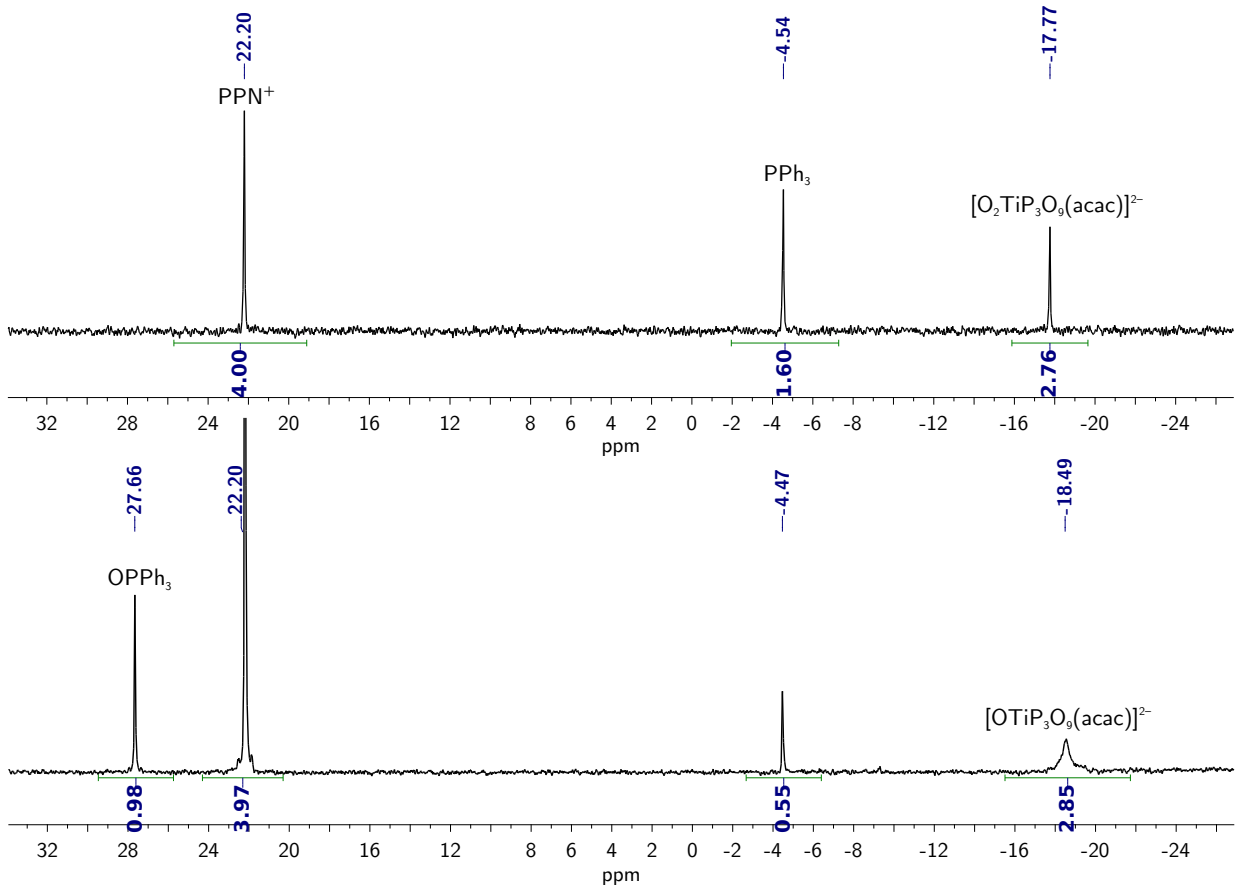

Figure S48: $^{31}P\{^1H\}$ NMR spectra of a solution of $[PPN]_2$[**4**] after treatment with 1.5 eq PPh_3 at 23 °C after 30 sec (top), and after 1 h at 70 °C (bottom) (MeCN, 121 MHz, 25 °C).

13 Experiments testing the catalytic activity of 1 and 2 towards organic substrates in the presence of H_2O_2.

The conditions used for these reactions were adapted from literature procedures for similar transformations.[4] General procedure for phenol, *cis*-cyclooctene, and diphenylmethanol substrates: In the fumehood, colorless solutions of $[PPN]_4$[**1**] (10 mg, 0.0034 mmol, 1.0 eq) and $[PPN]_2$[**2**] (10 mg, 0.0068 mmol, 1.0 eq) were prepared in CD_3CN (0.5 mL). To these solutions was added each substrate (2 eq per Ti center). After allowing complete dissolution of the substrate, urea H_2O_2 (20 eq per Ti center) was added to each solution as a solid. The colors of the solutions gradually became orange, and then ^1H and $^{31}P\{^1H\}$ NMR spectra of these reaction mixtures were collected after 20 min at 23 °C. ^1H and $^{31}P\{^1H\}$ NMR spectra of the reaction mixtures were checked again after 2 additional h at 23 °C. No new organic products were observed in the ^1H NMR spectra, so the solutions were heated at 70 °C for 4 h and checked again. The ^1H NMR spectra did not contain resonances corresponding to any new organic products, and the $^{31}P\{^1H\}$ NMR spectra all displayed resonances associated with the peroxotitanium metaphosphate complexes **3** and **4**.

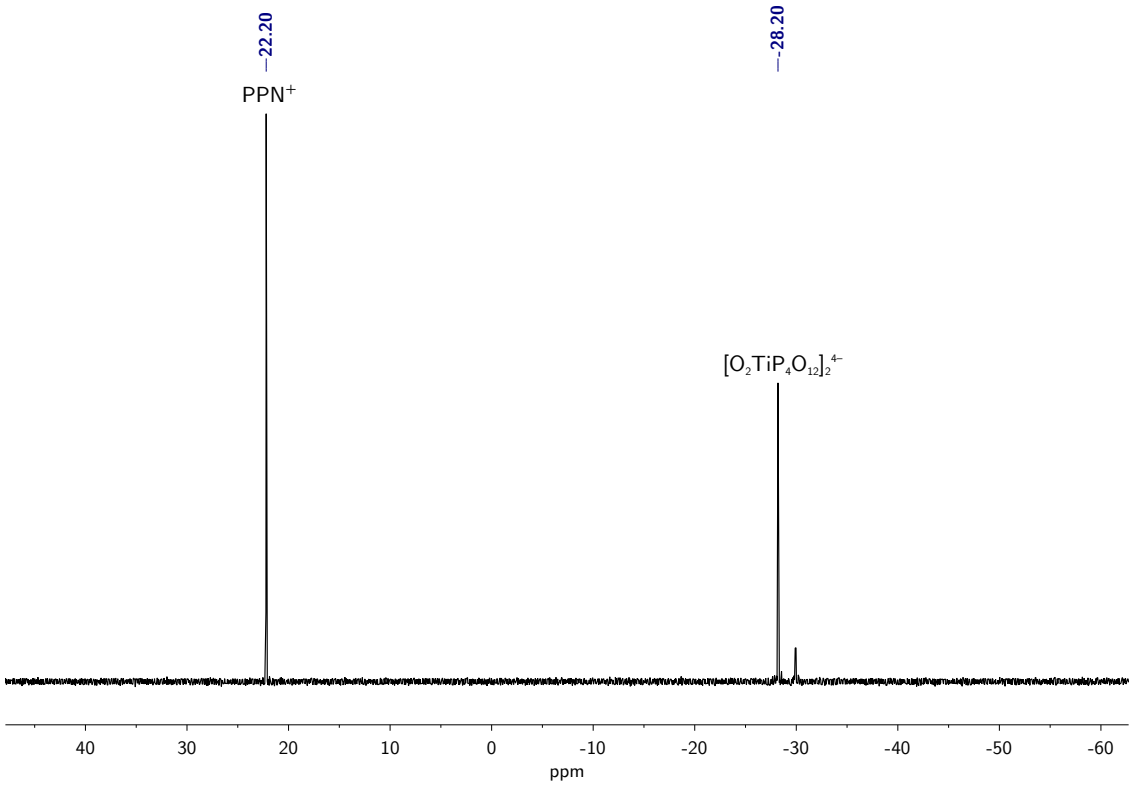

Figure S49: $^{31}P\{^{1}H\}$ NMR spectrum of the reaction of a solution of **1** + phenol + UHP after heating at 70 °C for 4 h (CD_3CN, 121 MHz, 25 °C).

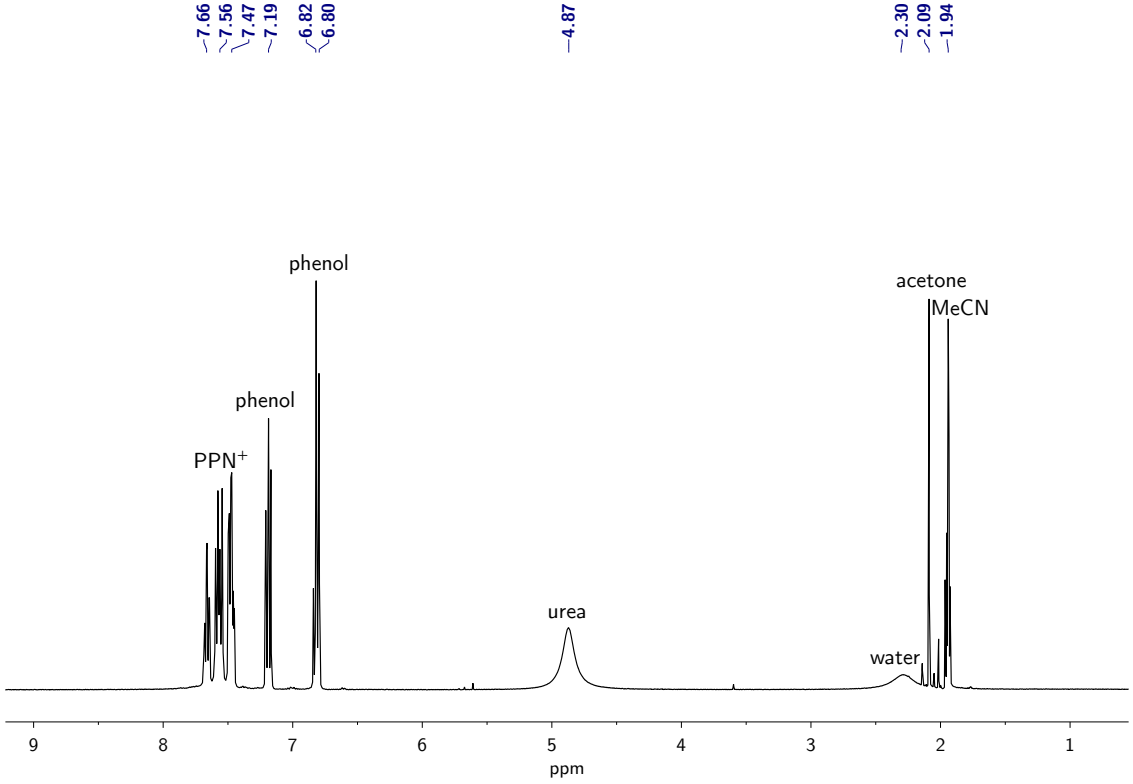

Figure S50: ^{1}H NMR spectrum of the reaction of a solution of **1** + phenol + UHP after heating at 70 °C for 4 h (CD_3CN, 400 MHz, 25 °C). Only urea, PPN^+ and phenol resonances are observed.

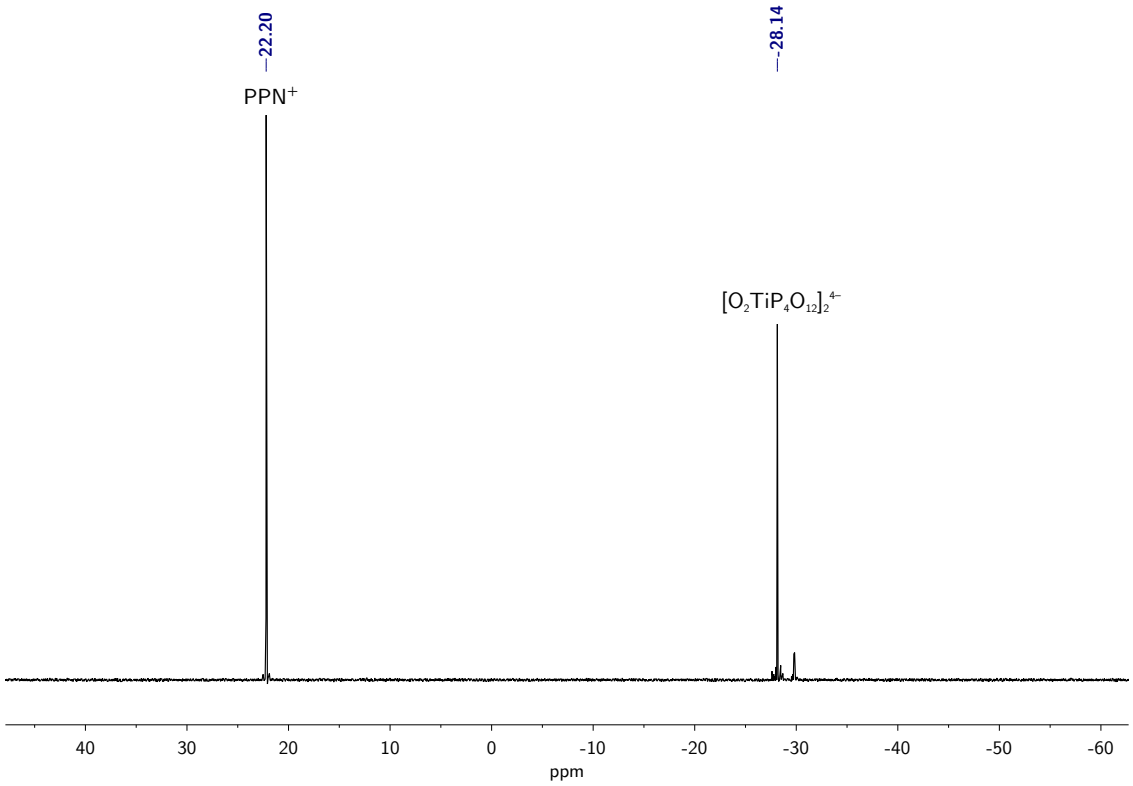

Figure S51: $^{31}P\{^{1}H\}$ NMR spectrum of the reaction of a solution of **1** + diphenylmethanol + UHP after heating at 70 °C for 4 h (CD_3CN, 121 MHz, 25 °C).

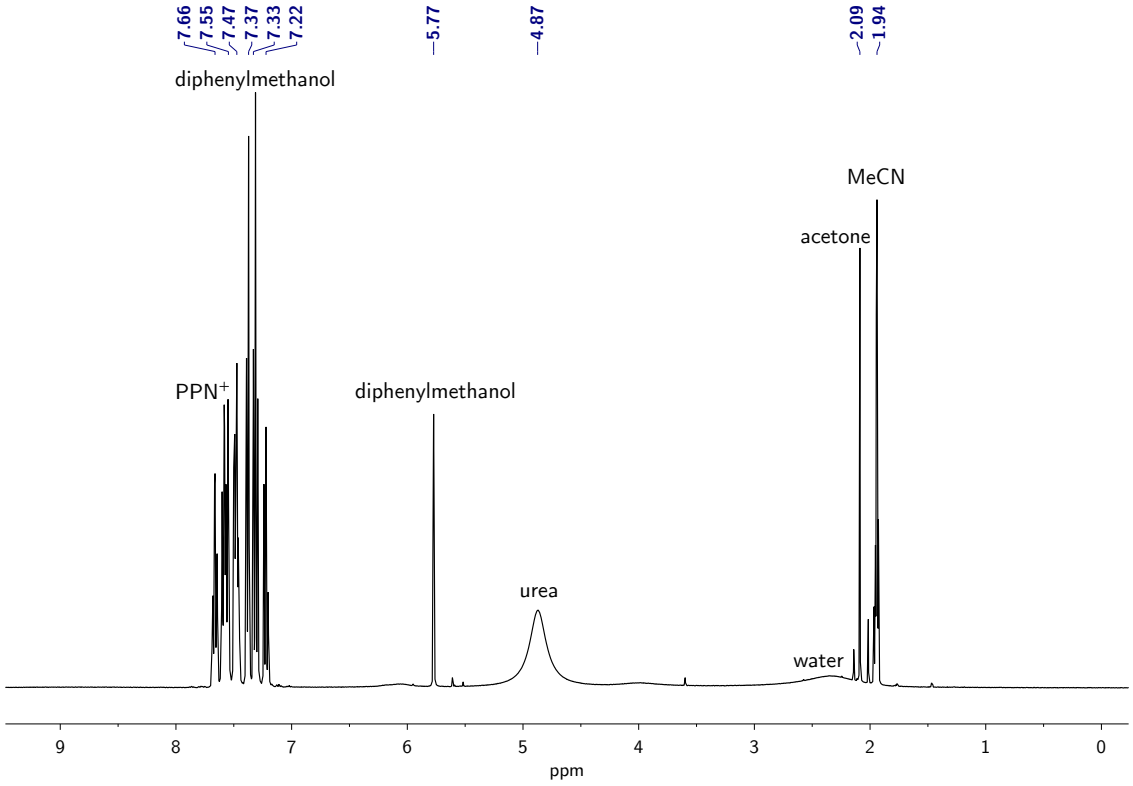

Figure S52: ^{1}H NMR spectrum of the reaction of a solution of **1** + diphenylmethanol + UHP after heating at 70 °C for 4 h (CD_3CN, 400 MHz, 25 °C). Only urea, PPN^+ and diphenylmethanol resonances are observed.

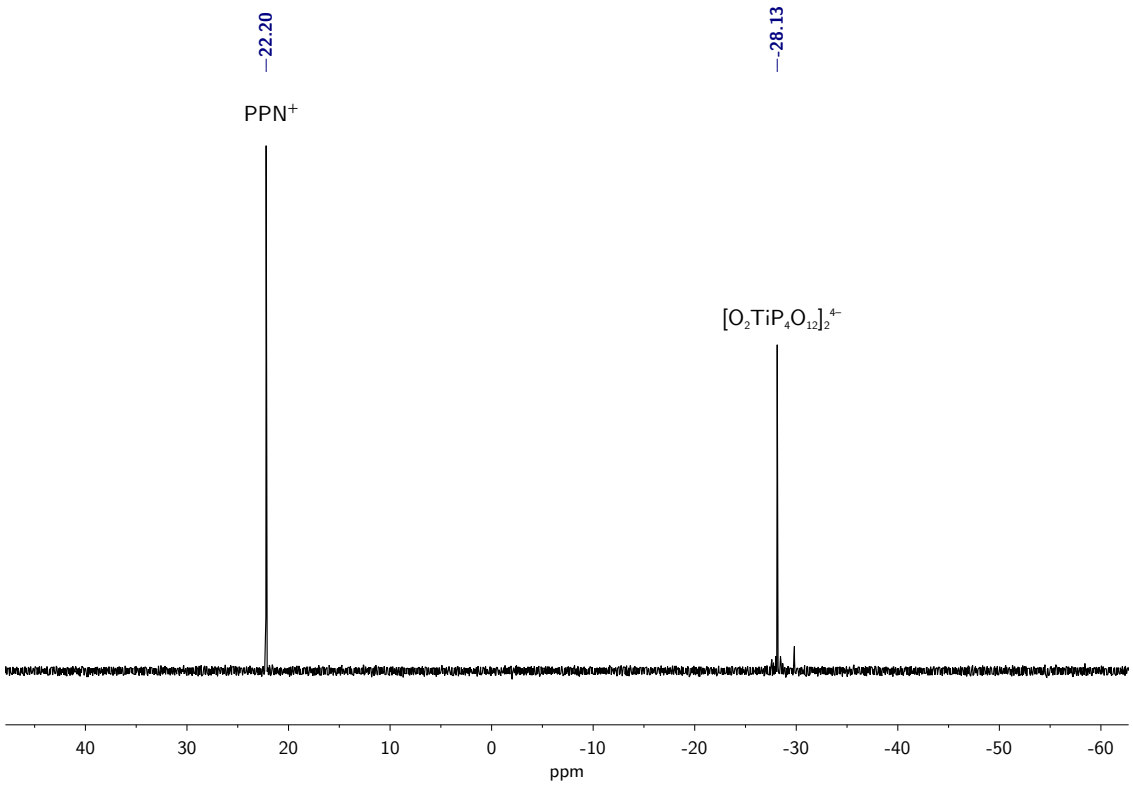

Figure S53: $^{31}P\{^{1}H\}$ NMR spectrum of the reaction of a solution of **1** + *cis*-cyclooctene + UHP after heating at 70 °C for 4 h (CD_3CN, 121 MHz, 25 °C).

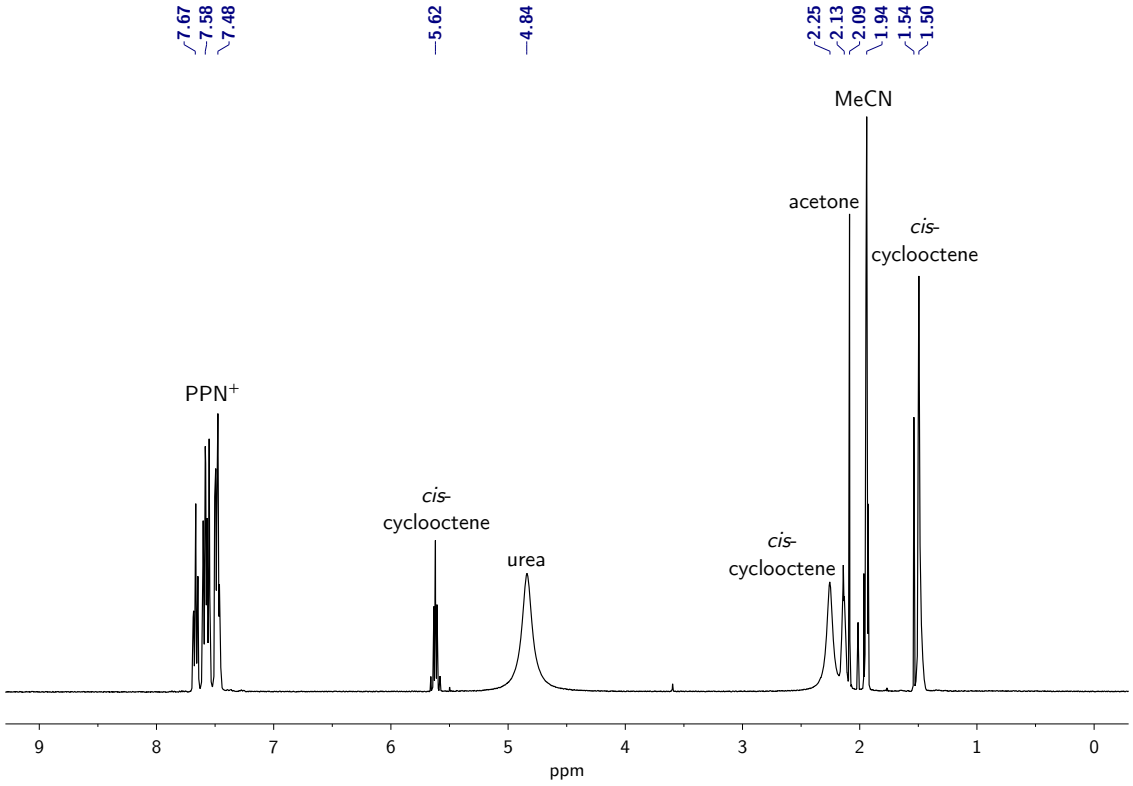

Figure S54: ^{1}H NMR spectrum of the reaction of a solution of **1** + *cis*-cyclooctene + UHP after heating at 70 °C for 4 h (CD_3CN, 400 MHz, 25 °C). Only urea, PPN^+ and *cis*-cyclooctene resonances are observed.

14 Experiments testing the oxidizing capacity of 3 and 4 towards organic substrates.

General procedure for phenol, *cis*-cyclooctene, and diphenylmethanol substrates:

In the fumehood, orange solutions of $[PPN]_4$[**3**] (10 mg, 0.0034 mmol, 1.0 eq) and $[PPN]_2$[**4**] (10 mg, 0.0068 mmol, 1.0 eq) were prepared in CD_3CN (0.5 mL). To these solutions was added each substrate (1 eq per Ti center). ^1H and $^{31}P\{^1H\}$ NMR spectra of these reaction mixtures were collected after 20 min at 23 °C. ^1H and $^{31}P\{^1H\}$ NMR spectra of the reaction mixtures were checked again after 2 additional h at 23 °C. No new organic products were seen in the ^1H NMR spectra, so the solutions were heated at 70 °C for 4 h. ^1H NMR analyses of these reaction mixtures after heating did not show the presence of any new organic products, and the $^{31}P\{^1H\}$ NMR spectra all displayed resonances associated with the peroxotitanium metaphosphate complexes **3** and **4**.

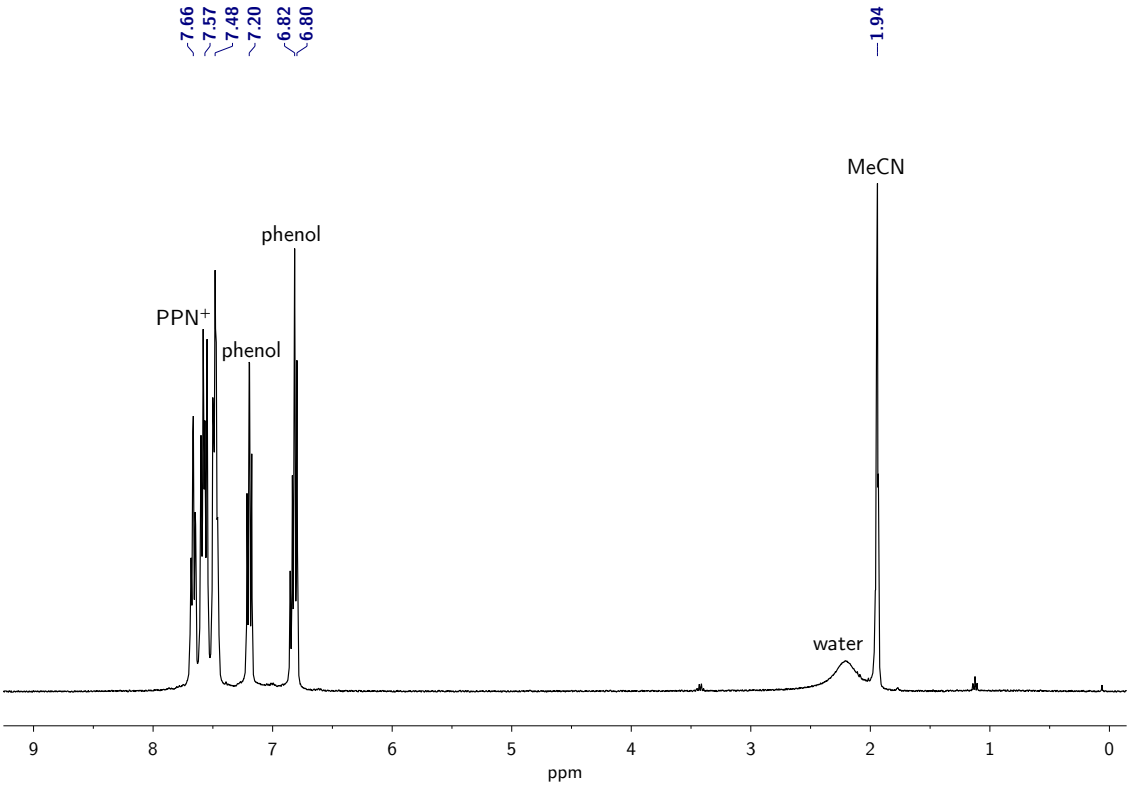

Figure S55: ^1H NMR spectrum of the reaction of a solution of **3** + phenol after heating at 70 °C for 4 h (CD_3CN, 400 MHz, 25 °C). Only PPN^+ and phenol resonances are observed.

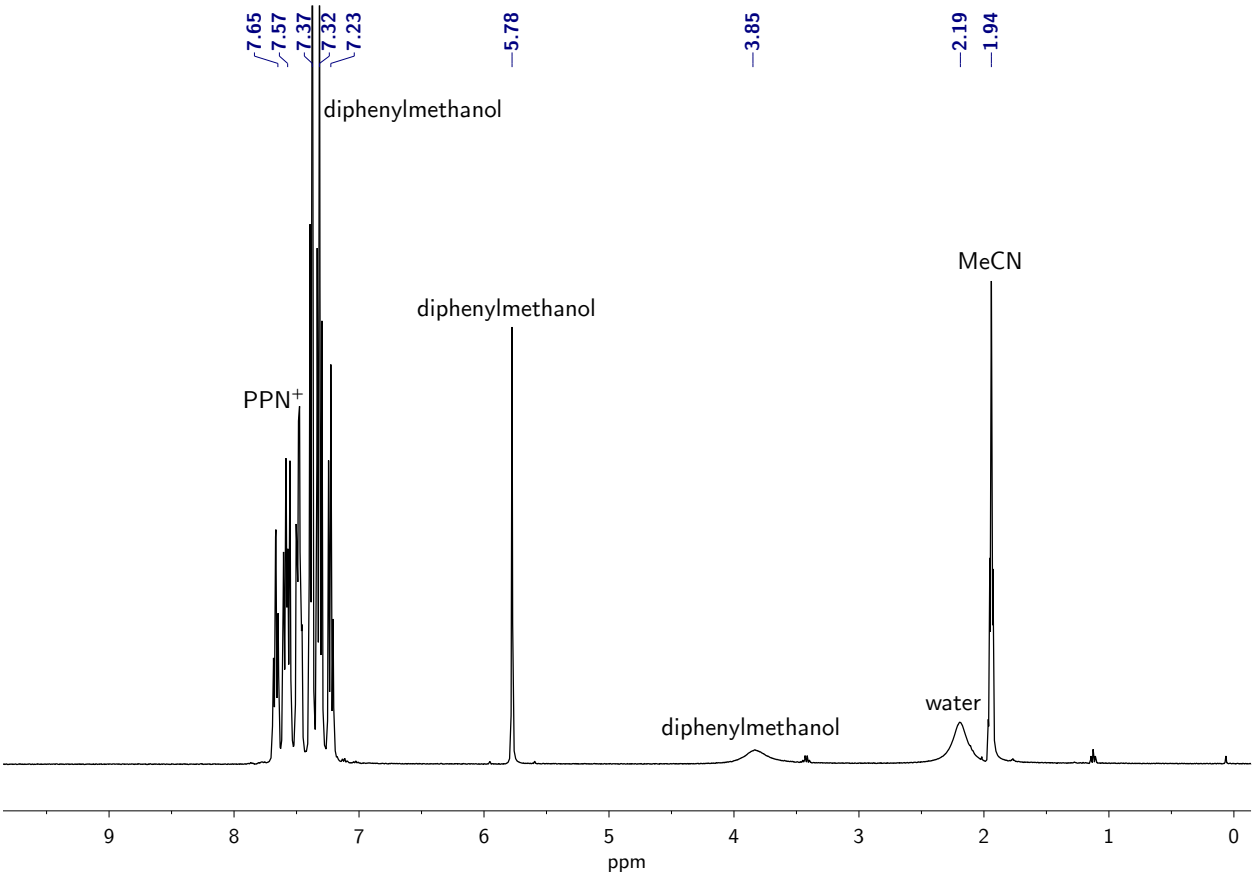

Figure S56: ^{1}H NMR spectrum of the reaction of a solution of **3** + diphenylmethanol after heating at 70 °C for 4 h (CD_3CN, 400 MHz, 25 °C). Only PPN^+ and diphenylmethanol resonances are observed.

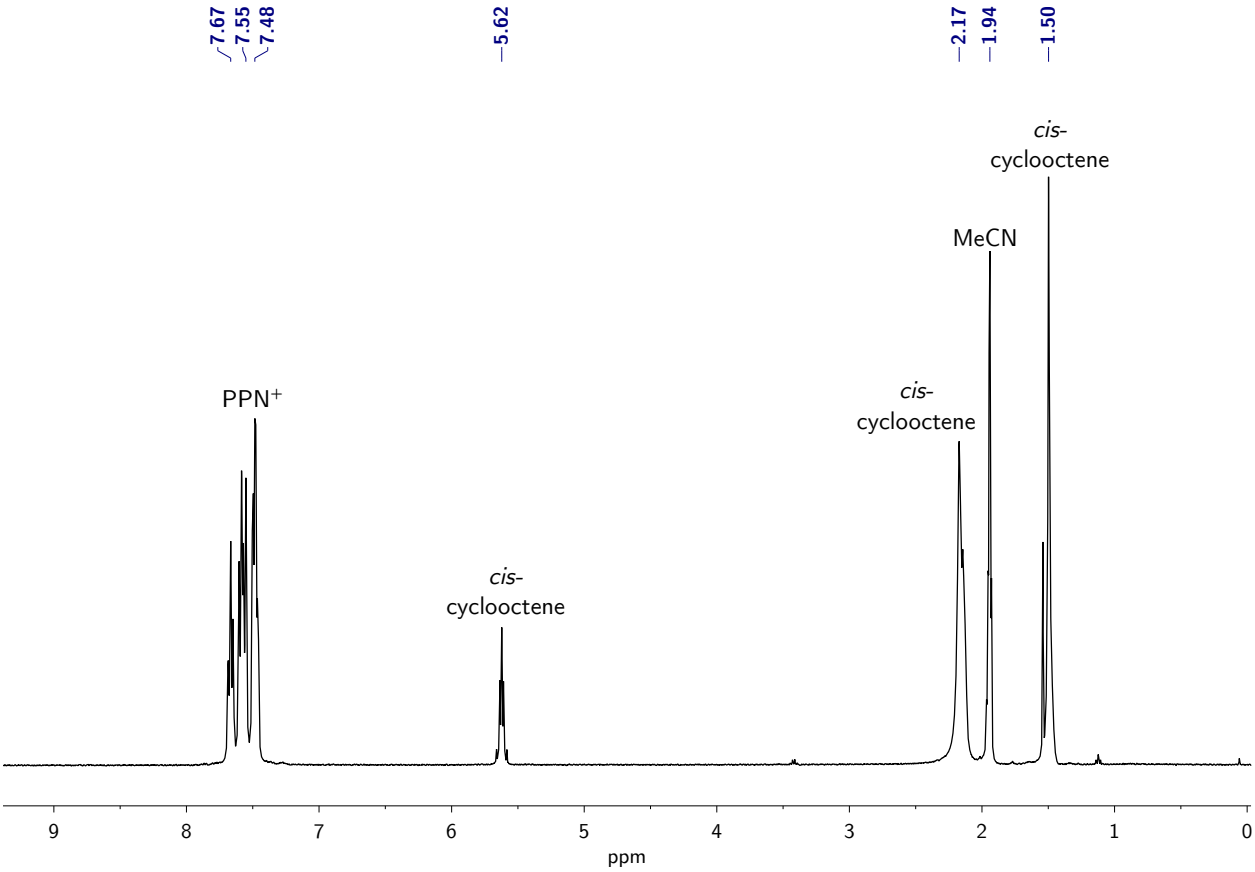

Figure S57: ^{1}H NMR spectrum of the reaction of a solution of **3** + *cis*-cyclooctene after heating at 70 °C for 4 h (CD_3CN, 400 MHz, 25 °C). Only PPN^+ and *cis*-cyclooctene resonances are observed.

15 Crystallographic information for $[PPN]_4$[1], $[PPN]_2$[2], $[PPN]_4$[3], and $[PPN]_2$[4].

15.1 X-ray crystal structure determination details.

Low-temperature (100 K) diffraction data (ϕ and ω) were collected on a Bruker-AXS X8 Kappa Duo diffractometer coupled to a Smart APEX2 CCD detector with Mo Kα radiation (λ = 0.71073 Å) from an IμS micro-source. Absorption and other corrections were applied using SADABS.[5] The structures were solved by direct methods using SHELXT[6] and refined against F^2 on all data by full-matrix least squares with SHELXL-2015[7] using established refinement approaches.[8] All hydrogen atoms were included into the model at geometrically calculated positions and refined using a riding model. The isotropic displacement parameters of all hydrogen atoms were fixed to 1.2 times the U_{eq} value of the atoms they are linked to (1.5 times for methyl groups). Details about crystal properties, diffraction data and crystal structures can be found in the tables below. All disorders were refined with the help of similarity restraints on 1,2- and 1,3-distances as well as similar ADP and advanced rigid bond restraints.[9]

The program SQUEEZE[10] as implemented in PLATON[11] was used to account for the contribution of disordered solvent contained in voids within the crystal lattice for structures $[PPN]_2$[**1**], $[PPN]_4$[**3**], and $[PPN]_2$[**4**]. The solvent contribution was added to the model in a separate file (the .fab file) by SHELXL.

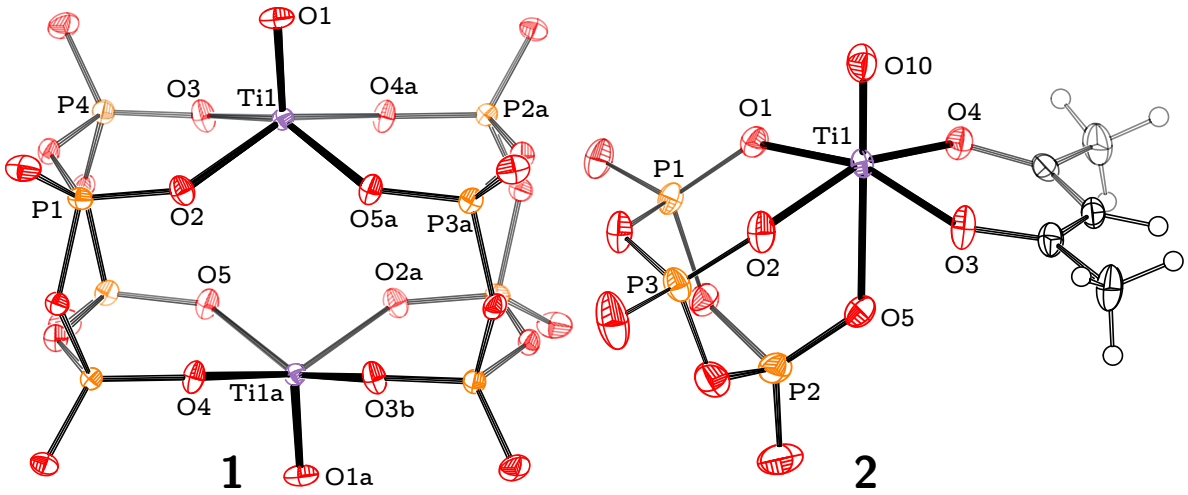

Figure S58: Solid-state structures of $[OTiP_4O_{12}]_2^{4-}$ (**1**, left) and $[OTiP_3O_9(acac)]^{2-}$ (**2**, right) rendered with PLATON[12] with thermal ellipsoids at the 50% probability level, and with $[PPN]^+$ cations and solvent molecules of crystallization omitted for clarity. Selected interatomic distances (Å) and angles (°): **1**, Ti1-O1 1.6252(13), Ti1-O2 1.9909(12), Ti1-O3 1.9939(13), Ti1-O4a 1.9844(13), Ti1-O5a 2.0014(13), Ti1-Ti1a 4.233(9), $\Sigma(O_{eq}\text{-Ti-}O_{eq})$ 341.8(9); **2**, Ti1-O10 1.644(2), Ti1-O1 2.033(2), Ti1-O2 2.0491(18), Ti1-O3 2.0145(19), Ti1-O4 2.0113(19), Ti1-O5 2.3211(19), $\Sigma(O_{eq}\text{-Ti-}O_{eq})$ 355.08(2).

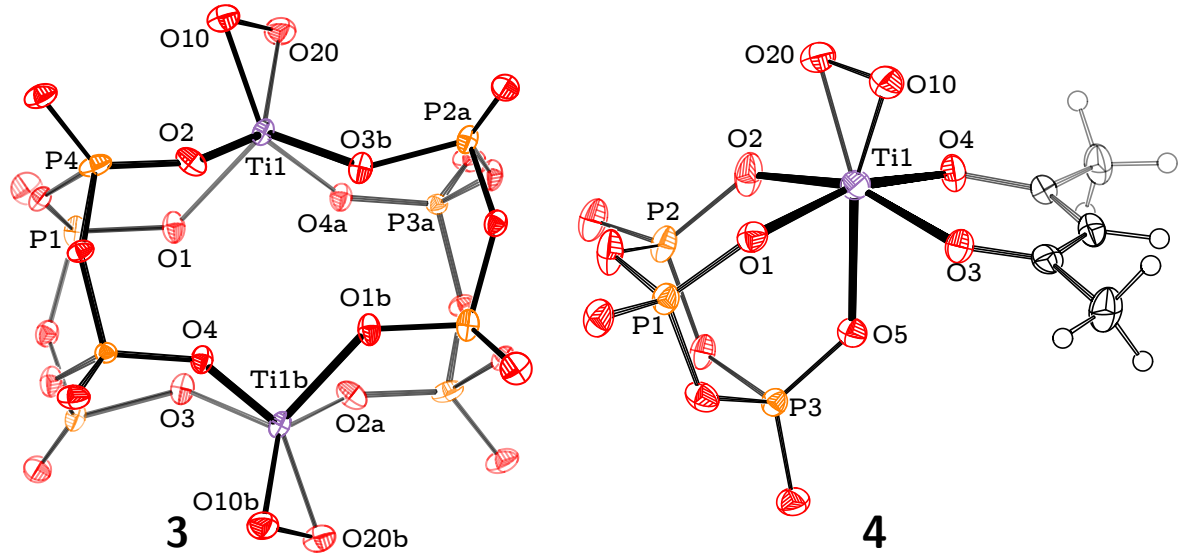

Figure S59: Solid-state structures of $[O_2TiP_4O_{12}]_2^{4-}$ (**3**, left) and $[O_2TiP_3O_9(acac)]^{2-}$ (**4**, right) rendered with PLATON[12] with thermal ellipsoids at the 50% probability level, and with $[PPN]^+$ cations and solvent molecules of crystallization omitted for clarity. Selected interatomic distances (Å) and angles (°): **3**, Ti1-O10 1.815(8), Ti1-O20 1.795(8), Ti1-O1 1.896(13), Ti1-O2 1.935(12), Ti1-O3b 1.986(13), Ti1-O4a 1.963(12), O20-O10 1.486(6), Ti1-Ti1b 4.23(1), $\Sigma(O_{eq}\text{-Ti-}O_{eq})$ 352.0(7); **4**, Ti1-O20 1.850(4), Ti1-O10 1.823(5), Ti1-O1 2.063(3), Ti1-O2 2.048(2), Ti1-O3 2.040(2), Ti1-O4 1.997(2), Ti1-O5 2.166(2), O10-O20 1.443(6), $\Sigma(O_{eq}\text{-Ti-}O_{eq})$ 353.9(8).

Table 1: Crystallographic Data for $[PPN]_4[\mathbf{1}]$, and $[PPN]_2[\mathbf{2}]$

	$[PPN]_4[\mathbf{1}]$	$[PPN]_2[\mathbf{2}]$
Reciprocal Net code / CCDC	X8_14143 / 1519761	X8_14116 / 1519762
Empirical formula, FW (g/mol)	$C_{38.50}H_{34}N_{1.50}O_7P_4Ti_{0.5}$, 777.50	$C_{77}H_{67}N_2O_{12}P_7Ti$, 1477.01
Color / Morphology	Colorless / Block	Colorless / Block
Crystal size (mm^3)	$0.100 \times 0.080 \times 0.080$	$0.110 \times 0.100 \times 0.070$
Temperature (K)	100(2)	100(2)
Wavelength (Å)	0.71073	0.71073
Crystal system, Space group	Triclinic, $P\bar{1}$	Monoclinic, $P2_1$
Unit cell dimensions (Å, °)	a = 16.3690(11), α = 92.9790(10)	a = 10.714(2), α = 90
	b = 16.3925(11), β = 112.5450(10)	b = 12.719(2), β = 100.945(4)
	c = 17.2399(12), γ = 109.6980(10)	c = 27.457(5), γ = 90
Volume ($Å^3$)	3934.1(5)	3673.7(12)
Z	4	2
Density (calc., g/cm^3)	1.313	1.335
Absorption coefficient (mm^{-1})	0.335	0.335
$F(000)$	1610	1584
Theta range for data collection (°)	1.308 to 28.017	1.511 to 31.081
Index ranges	$-21 \leq h \leq 21$, $-21 \leq k \leq 21$,	$-15 \leq h \leq 15$, $-18 \leq k \leq 18$,
	$-22 \leq l \leq 22$	$-39 \leq l \leq 39$
Reflections collected	133174	135224
Independent reflections, R_{int}	18880, 0.0388	22707, 0.0484
Completeness to θ_{max} (%)	99.9	99.9
Absorption correction	Semi-empirical from equiv.	Semi-empirical from equiv.
Refinement method	Full-matrix least-squares on F^2	Full-matrix least-squares on F^2
Data / Restraints / Parameters	18880 / 1488 / 931	22707 / 1489 / 894
Goodness-of-fit[a]	1.034	1.035
Final R indices[b] $[I > 2\sigma(I)]$	$R_1 = 0.0382$, $wR_2 = 0.0993$	$R_1 = 0.0376$, $wR_2 = 0.0845$
R indices[b] (all data)	$R_1 = 0.0459$, $wR_2 = 0.1047$	$R_1 = 0.0494$, $wR_2 = 0.0895$
Largest diff. peak and hole ($e \cdot Å^{-3}$)	1.273 and −0.753	0.761 and −0.490

[a] GooF = $\sqrt{\frac{\Sigma[w(F_o^2-F_c^2)^2]}{(n-p)}}$ [b] $R_1 = \frac{\Sigma||F_o|-|F_c||}{\Sigma|F_o|}$; $wR_2 = \sqrt{\frac{\Sigma[w(F_o^2-F_c^2)^2}{\Sigma[w(F_o^2)^2]}}$; $w = \frac{1}{\sigma^2(F_o^2)+(aP)^2+bP}$; $P = \frac{2F_c^2+\max(F_o^2,0)}{3}$

Table 2: Crystallographic Data for $[PPN]_4$[**3**], and $[PPN]_2$[**4**]

	$[PPN]_4$[**3**]	$[PPN]_2$[**4**]
Reciprocal Net code / CCDC	X8_14131 / 1519760	X8_14133 / 1519759
Empirical formula, FW (g/mol)	$C_{156}H_{138}N_{10}O_{28}P_{16}Ti_2$, 3192.08	$C_{77}H_{67}N_2O_{13}P_7Ti$, 1493.01
Color / Morphology	Orange / Needle	Orange / Block
Crystal size (mm^3)	$0.360 \times 0.040 \times 0.040$	$0.070 \times 0.040 \times 0.040$
Temperature (K)	100(2)	100(2)
Wavelength (Å)	0.71073	0.71073
Crystal system, Space group	Triclinic, $P\bar{1}$	Monoclinic, $P2_1$
Unit cell dimensions (Å, °)	a = 16.299(4), α = 93.178(5)	a = 10.7436(17), α = 90
	b = 16.316(4), β = 112.261(4)	b = 12.8084(19), β = 100.464(3)
	c = 17.375(4), γ = 109.853(4)	c = 27.344(4), γ = 90
Volume ($Å^3$)	3931.1(17)	3700.2(10)
Z	1	2
Density (calc., g/cm^3)	1.348	1.340
Absorption coefficient (mm^{-1})	0.337	0.331
$F(000)$	1652	1548
Theta range for data collection (°)	1.296 to 26.438	1.515 to 26.406
Index ranges	$-20 \leq h \leq 20$, $-20 \leq k \leq 20$,	$-13 \leq h \leq 13$, $-16 \leq k \leq 16$,
	$-21 \leq l \leq 21$	$-34 \leq l \leq 34$
Reflections collected	160121	91080
Independent reflections, R_{int}	16072, 0.0419	15169, 0.0479
Completeness to θ_{max} (%)	99.9	100.0
Absorption correction	Semi-empirical from equiv.	Semi-empirical from equiv.
Refinement method	Full-matrix least-squares on F^2	Full-matrix least-squares on F^2
Data / Restraints / Parameters	16072 / 1927 / 1096	15169 / 1814 / 968
Goodness-of-fit[a]	1.088	1.020
Final R indices[b] [$I > 2\sigma(I)$]	$R_1 = 0.0381$, $wR_2 = 0.1072$	$R_1 = 0.0332$, $wR_2 = 0.0755$
R indices[b] (all data)	$R_1 = 0.0452$, $wR_2 = 0.1125$	$R_1 = 0.0396$, $wR_2 = 0.0787$
Largest diff. peak and hole ($e \cdot Å^{-3}$)	0.857 and −0.483	0.356 and −0.296

[a] GooF = $\sqrt{\frac{\Sigma[w(F_o^2-F_c^2)^2]}{(n-p)}}$ [b] $R_1 = \frac{\Sigma||F_o|-|F_c||}{\Sigma|F_o|}$; $wR_2 = \sqrt{\frac{\Sigma[w(F_o^2-F_c^2)^2}{\Sigma[w(F_o^2)^2]}}$; $w = \frac{1}{\sigma^2(F_o^2)+(aP)^2+bP}$; $P = \frac{2F_c^2+\max(F_o^2,0)}{3}$

References

(1) Ammann, C.; Meier, P.; Merbach, A. A Simple Multinuclear NMR Thermometer. *J. Magn. Reson.* **1982**, *46*, 319–321.

(2) (a) Wong, E. H.; Sun, X.; Gabe, E. J.; Lee, F. L.; Charland, J. P. Coordination Complexes Derived from Tri-, Tetra-, and Pentaphosphoxane Rings. *Organometallics* **1991**, *10*, 3010–3020; (b) Sun, X.; Wong, E. H.; Turnbull, M. M.; Rheingold, A. L.; Waltermire, B. E.; Ostrander, R. L. Metal-Assisted Formation of Phosphorus-Oxygen Heterocyclic Complexes. *Organometallics* **1995**, *14*, 83–97.

(3) (a) Rummey, J. M.; Boyce, M. C. Introducing the gNMR Program in an Introductory NMR Spectrometry Course To Parallel Its Use by Spectroscopists. *J. Chem. Educ.* **2004**, *81*, 762–763; (b) *gNMR, 4.0.1*; Cherwell Scientific Publishing Limited: Oxford, United Kingdom, 1995.

(4) (a) Liu, Q.-X.; Zhou, Z.-H. Monomeric Peroxo Titanate Coordinated with Cyclohexanediaminetetraacetate: Towards the Active Oxygen Species of the Ti(IV) Site Hosted in the Titanium Silicalite Catalyst TS-1. *Polyhedron* **2012**, *35*, 1–6; (b) Clerici, M. G. Oxidation of Saturated Hydrocarbons with Hydrogen Peroxide, Catalysed by Titanium Silicalite. *Appl. Catal.* **1991**, *68*, 249–261.

(5) Krause, L.; Herbst-Irmer, R.; Sheldrick, G. M.; Stalke, D. Comparison of Silver and Molybdenum Microfocus X-ray Sources for Single-Crystal Structure Determination. *J. Appl. Cryst.* **2015**, *48*, 3–10.

(6) Sheldrick, G. M. *SHELXT* – Integrated Space Group and Crystal Structure Determination. *Acta Crystallogr. A* **2015**, *71*, 3–8.

(7) Sheldrick, G. M. Crystal Structure Refinement with *SHELXL*. *Acta Crystallogr. C* **2015**, *71*, 3–8.

(8) Müller, P. Practical Suggestions for Better Crystal Structures. *Crystallogr. Rev.* **2009**, *15*, 57–83.

(9) Thorn, A.; Dittrich, B.; Sheldrick, G. M. Enhanced Rigid-bond Restraints. *Acta Crystallogr. A* **2012**, *68*, 448–451.

(10) van der Sluis, P.; Spek, A. L. BYPASS: An Effective Method for the Refinement of Crystal Structures Containing Disordered Solvent Regions. *Acta Crystallogr. A* **1990**, *46*, 194–201.

(11) Spek, A. L. Structure Validation in Chemical Crystallography. *Acta Crystallogr. D* **2009**, *65*, 148–155.

(12) Spek, A. L. author. *Acta Cryst.* **2009**, *D65*, 148–155.